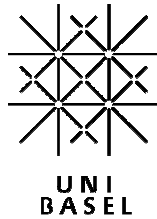# Controlled Self-Assembly of Short β-helical Peptides

UNI
BASEL

Inauguraldissertation

zur

Erlangung der Würde eines Doktors der Philosophie

vorgelegt der Philosophisch-Naturwissenschaftlichen Fakultät der

Universität Basel

von

Christian Dittrich

aus Deutschland

Genehmigt von der Philosophisch-Naturwissenschaftlichen Fakultät auf Antrag von

Prof. Dr. Wolfgang Meier (Universität Basel)
und
Prof. Dr. Andreas Taubert (Universität Potsdam & MPI für Kolloid- und Grenzflächenforschung)

Basel, den 13. März. 2007

Prof. Dr. Hans-Peter Hauri
Dekan

To my Family

and

Simone

Acknowledgements

This thesis was performed between October 2003 and March 2007 in the department of chemistry at the University of Basel. I wish to acknowledge the following persons who contributed considerably to this work:

Prof. Dr. Wolfgang Meier, for supervising my thesis, giving me all the freedom to do my own mistakes and helping me to grow up as a scientist.

Prof. Dr. A. Taubert, for corefering this thesis and good discussions.

Prof. Dr. H. Huber, for the time he sacrificed to preside my Ph.D. defense.

Dirk de Bruyn, for his scientific enthusiasm, all the great discussions and for introducing his industrial experience about peptide chemistry to our group.

Sven Kasper, for his support with peptide synthesis, purification and characterization. Special thanks for his patience on the CD machine.

Dr. Katarzyna Kita, for hours and hours of interesting discussions, for helping me understand surface science, for teaching me how to clean Teflon troughs but most importantly for being a very good friend.

Dr. Roman Trojer, for being an excellent friend and setting me straight whenever it was necessary.

Additionally, I want to thank the whole Meier group for many great moments within the past three years.

1 Abstract

Cells as functional units from algae to mammals demonstrate the most remarkable degree of self-organization. Processes like membrane formation, protein folding and signal cascades excel in selectivity and control. Nanotechnology is often inspired by biological properties but, despite Nature's seductive elegance and putative simplicity, often fails at prediction of complex self-assembly. Even weak forces, multiplied by the large number of subunits, contribute to the assemblies and frequently lead to unforeseen results. Membranes are prominent and well understood examples for self-organization and since there is a rising interest in vesicular self-assemblies, the number of potential applications increased with the complexity of the membrane material. The controlled variation of structure and dimension in supramolecular assemblies is a desirable feature for medical and technical applications. From lipids to polymers to the incorporation of proteins: today we are able to tailor membrane properties desirable for many purposes.

Highly specific interactions in between membrane constituents are a desirable feature. And when it comes to the discipline of self-assembly, barely a process compares to the specificity and control that is represented by proteins folding into their biologically active state. Thus, it is tempting to exploit this specificity not only in terms of *intra*molecular but also *inter*molecular interactions. However, the controlled formation of a membrane from short peptides has not been accomplished to this day.

The aim of this work was to construct membranes from peptides, shorter than 30 amino acids in primary structure. The main challenge of the project is the hydrophilic contribution of every amino acid's backbone that usually constrains the hydrophobic property of peptides. As a consequence, we considered secondary structure as the key to the formation of an entirely peptidic membrane constituent, an assumption that was confirmed by the helical conformation of the antibiotic peptide gramicidin. We present the formation of membranes based on its secondary structure motif and complemented it with varying lengths of positively charged oligo-lysine. The functional property of membrane formation could be assigned to the last seven amino acids of the gramicidin sequence, which allowed us to construct membranes out of peptides only eight amino acids in length. The results are unpreceded both in terms of controlled peptide self-assembly as well as abstraction from the peptides' biological purpose.

2 Introduction

2.1 Self-Assembly

Even though "self-assembly" is allegedly susceptible in the everyday lab work, it appears to be virtually impossible to define a principle that becomes evident in such a wealth of different manifestations. It emerges quickly that "self-assembly" as a term is too general to confine itself and consequently compares to universally applicable (and therefore meaningless) concepts like the "homo oeconomicus" or the increasingly popular interpretation of cultural and psychological phenomena by the theory of evolution.

The attempt to define "self-assembly" requires a constraint in subject matter that emerges when it is explained from the perspective of different scientific disciplines: physicists perceive self-assembly in terms of phenomena like ferromagnetism, superconductivity or convection cells and define it as a spontaneous formation of new three-dimensional and temporal structures in complex systems which results from the cooperative effect of partial systems. In chemistry, we talk about self-assembly when we think of well-defined structures like micelles and liquid crystals or oscillating reactions that spontaneously result from the components of a system. In biology again, self-assembly is observed in aspects like protein folding, formation of lipid double layers or morphogenesis which correspond to a spontaneous building-up of complex structures that take place under adequate environmental conditions without the effect of external factors.[1]

According to these examples, the use of the term "self-assembly" is often limited to processes that involve pre-existing components, are reversible and can be controlled by proper design of the components. As a consequence of this description, "self-assembly" is not equal to "formation".

Furthermore, we can generally distinguish two categories of self-assembled systems: static and dynamic. Static systems require energy to form but once their order is established they are in global or local thermodynamic equilibrium and do not dissipate more energy: lipid membranes, liquid crystals or most of the folded proteins for instance are in static equilibrium. Generally speaking, most of the research dedicated to self-assembly has been focused on this type.

By contrast, dynamically self-assembled systems (convection cells, oscillating reactions) are constantly dissipating energy and far away from thermodynamic equilibrium. Such dynamic instabilities result in the formation of ordered, so-called

dissipative structures; biological cells are an excellent example for the constant requirement of energy to maintain their structures and the ongoing interactions between their components. The fundamental understanding of dynamic self-assembly is still in its infancy and possibly requires new approaches to further elucidate them.[2]

Within the past decade scientists took steps towards control of artificially designed molecular self-organization. The size of these self-organized objects is often in the nanometer to micrometer range and thus, associated to the field of nanotechnology. The Journal of Nanotechnology describes the discipline in its scopes as "the field that attempts to individually address, control, and modify structures, materials and devices with nanometre precision, and the synthesis of such structures into systems of micro- and macroscopic dimensions."

There are generally two approaches to the fabrication of nanometer scaled systems: bottom-up and top-down. Whereas a boat can be made from a hollowed out tree (top-down) it is also possible to assemble it from smaller units like planks (bottom-up). Nature demonstrates impressive bottom-up design by processes like the formation of a membrane, the folding of a protein and its subsequent function as well as signal cascades, which all excel in selectivity and control. Chemical synthesis allows us to produce appropriate building blocks capable of self-assembling into larger ensembles like colloids, vesicles or nanotubes by the bottom-up approach. However, nanotechnology is frequently inspired by biological properties but, despite nature's seductive simplicity and elegance, often fails at the prediction of complex self-organisation; even weak forces, multiplied by the assembly's large number of subunits, contribute to the formation and frequently lead to unforeseen results.

The subsequent sections of the first chapter briefly summarize the self-assembly properties of membranes and proteins. Whereas the formation of a regular membrane structure depends largely on the intermolecular interactions of the constituents, proteins organize their three dimensional structure which can be considered as intramolecular self-assembly. Both processes matter to the topic of this work.

2.1.1 *Membrane Formation*

The common feature of all membrane constituents is the presence of both a hydrophilic block (A) and hydrophobic block (B) in the molecular structure (Figure 1).

This specificity allows for dissolution of the hydrophobic fragments in a non-polar environment, whereas the hydrophilic groups will have high affinity to the polar (aqueous) medium.[3]
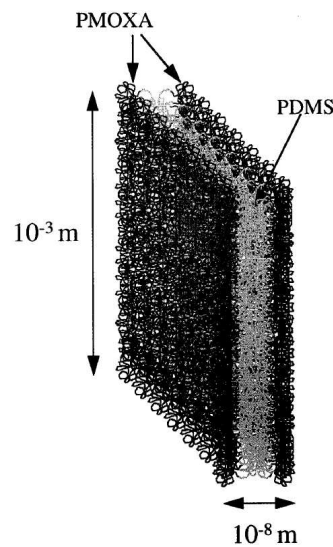

Figure 1 Structure of a membrane. In this example, the hydrophilic block A is represented by poly-(2-methyloxazoline) and the hydrophobic block B consists of poly(dimethylsiloxane).[4]

Self-assembly of a membrane can take place when long range repulsive as well as short range attractive forces are involved: considering the structure of an amphiphilic molecule, the intermolecular repulsive interactions take place between blocks of opposite polarity (A, hydrophilic) and (B, hydrophobic) whereas the short range attractive forces (covalent bonds) simply hold together block A and block B. The entropy difference of the solvent (usually water) as a response to the interaction with block A and block B contributes to the self-assembly as well, and leads to a maximized contact area between blocks of identical polarity with as few contacts as possible with the opposite block.

Presently, membranes can be prepared from phospholipids[5], surfactants [6] and block copolymers.[4] Role model of all artificially established membrane systems is the biological cell membrane. Its underlying structure is based on seemingly simple ingredients, yet its material properties supporting basic life functions remain an inspiration to modern science. Due to a rising economical interest in artificial vesicular systems, biological and artificial membranes are among the best studied systems in the field of molecular self-assembly and it is very desirable to introduce functionality by construction of hybrid membrane materials[7-10] or to construct membranes consisting of purely bioactive compounds.[11]

2.1.2 *Protein Folding*

In order to accomplish their biological tasks, proteins need to adopt characteristic functional shapes, also denoted as the native state. The folding reaction involves a complex intramolecular process which depends on the cooperative action of disulfide bonds in addition to many relatively weak nonbonding interactions such as Van der Waals-forces, π-π interactions as well as hydrogen-bonds. Nature benefits from the diversity by formation of secondary, tertiary and quaternary protein structures that exhibit reproducible folds and precise positioning of functional groups. Amino acids far apart in the primary sequence can be brought to close proximity in the three-dimensional space for example to form the active site of enzymes.

Due to steric hindrance, protein backbones prefer to adopt discrete secondary structure motifs, which involves the rotation of the bonds on either side of the α-carbon.
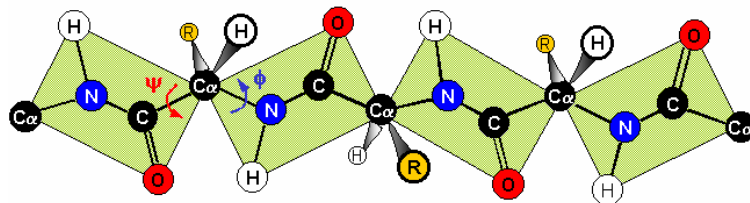
Figure 2 General structure of a peptide (from: http://employees.csbsju.edu/hjakubowski)

The angle of rotation around the N-C_α bond is denoted Φ and the one around the C_α-C bond is called Ψ (Figure 2). In an element of secondary structure, all the Φ- and Ψ-values are approximately the same, which results an ordered structure. Sterically forbidden conformations are those in which any nonbonding interatomic distance is smaller than the corresponding van der Waals distance. Secondary structure information is summarized in a Ramachandran plot (Figure 3) and with a realistic set of Φ and Ψ values, there are mainly three small regions of the conformational map that are physically accessible to a polypeptide chain, giving rise to three distinct types of secondary structure: the α-helix, the β-strand and the β-turn. The reverse reaction of the folding process is called denaturation or misfolding where the native structure of a protein is disrupted and a random coil ensemble of unfolded structures is formed instead: boiling an egg results in denaturation of proteins, which, in this case, is irreversible since cooling it down again does not restore their original appearance.

Denaturation can be carried out chemically by the addition of denaturants like urea or thermally by heating (and sometimes cooling). Some denatured proteins can refold however, in many cases denaturation is irreversible.
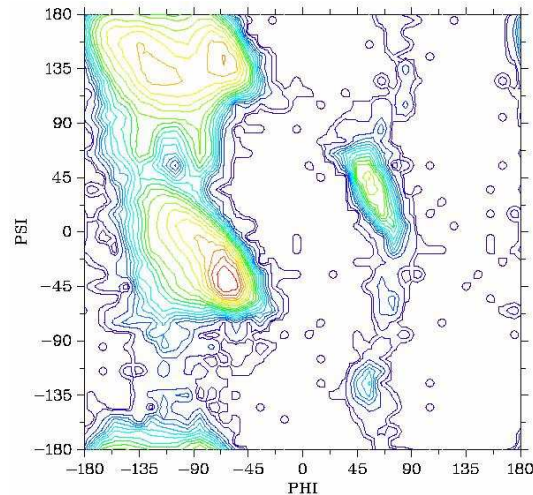

Figure 3 A Ramachandran plot describes the occurrence of Φ and Ψ angles in a given protein (from: http://gchelpdesk.ualberta.ca)

But how does a protein fold to its native conformation? Indeed the number of possible structures for a polypeptide chain is astronomically large, a "permutational" search for the native state would require an almost infinite length of time. It is virtually impossible that folding processes can occur by random search of the protein's conformational space.

Anfinsen[12] considered the possibility that "templates" somehow caused proteins to assume their native conformation but even if that was true, one would still have to explain how the template achieved its conformation. Yet, many proteins fold to their native state in less than a few seconds and therefore, Levinthal[13] proposed that proteins must form structure in a time-ordered sequence of events, called a "pathway". The nature of these events was left unexplained and it was unknown whether they are restricted to "native contacts" (defined as contacts that are preserved in the final structure), whether they might include non-specific interactions, such as a general collapse in size at the very beginning, or whether there are non-native but specific contacts. For the time being, methods have been developed to gain quantitative information about thermodynamic (isothermal titration calorimetry) and kinetic (stopped flow circular dichroism) properties of folding processes. Additionally, the "Φ-value analysis" links incremental structural variations

(introduction of point mutations) to physicochemical data and allows insight to the transition state of folding.

It becomes evident that the discipline of protein folding matters when it comes to a quantitative analysis of self-assembly processes and promises deepened understanding of its fundamental principles. Moreover, the structural and functional properties of proteins also provide insight to the potential control of intermolecular peptide interactions and hence open new perspectives for structural and functional macromolecular properties.

2.2 Previous Work on Peptide Self-Assembly

This part of the introduction is arranged according to the material properties of amphiphiles consisting of or containing peptides or proteins.

An interesting feature of peptide/polymer hybrids is the way of connecting both blocks. There is a multitude of ways to attach a synthetic hydrophobic polymer such as poly(butadiene) (PDB)[14, 15] poly(ethylene oxide) (PEG)[16, 17] or poly(styrene) (PS)[9] to a peptide or protein depending on the available chemical and structural properties.

An example for quite an exotic membrane forming hybrid is presented by Velonia et al. [9]; Lipase B from Candida Antarctica, a 33 kDa enzyme that catalyses the hydrolysis of esters was used as a huge hydrophilic head region and connected to maleimide functionalized polystyrene (n = 40) to induce amphiphilicity. The bond between hydrophilic and hydrophobic block was established via a single reduced disulfide bridge exposed to the outer surface of the protein. The coupling reaction between nonaggregated components was carried out in a 90 % THF solution. As indicated by Langmuir compression isotherm measurements the resulting amphiphiles were forming monolayers at the air-water interface (lift-off area = 28 nm^2). Formation of biohybrids was further verified by TEM pictures that revealed the presence of well-defined µm long fibers built up from bundles of rods, with the smallest rod having a diameter between 25 and 30 nm. This corresponds to the predicted micellar architecture diameter according to Israelachvilli's rules.[18]

A versatile system to combine peptides and polymers to form amphiphilic structures was demonstrated by Boerakker et al. [19]. They describe the construction of a giant amphiphile by direct coupling of a hydrophobic polymer (PS, n = 90) to a redox

13

enzyme by cofactor reconstitution. Horseradish peroxidase (HRP) was chosen since it contains a cofactor (ferriprotoporphyrin IX) which can easily be modified with hydrophobic chains on its carboxylic acid functional groups. Thus, the position of the conjugation site is precisely known. It is presumed that the polystyrene modified cofactor forms aggregates onto which apo-HRP can be reconstituted. This very large amphiphile of about 63 kDa tends to form vesicular structures in solution. Further evidence was provided for vesicular structures as 4(5)-carboxyfluorescein was included in the aggregates and released due to changes of the surrounding osmotic pressure. It is assumed that most proteins lose their function in a nonnatural environment. Interestingly, the aggregates still retain some enzymatic activity when reconstituted at 28 °C in potassium phosphate buffer at pH 7.5. Longer reconstitution times resulted in a decreased activity. Since proteins are generally more stable at lower temperatures, this behavior can be explained by thermal denaturation.

Unlike aforementioned example of hybrid amphiphiles, the work of Kimura and coworkers [16] establishes amphiphilicity by using the polymer PEG as the hydrophilic block and gramicidin A, a 15-mer-peptide antibiotic, as hydrophobic block. gramicidin A, composed entirely of hydrophobic amino acids is known to form helical ion channels in the hydrophobic core of lipid bilayers. By connecting a PEG chain as hydrophilic part to the C terminus through a urethane bond, the hydrophobic peptide is converted to an amphiphile. Circular dichroism measurements of gramicidin A-PEG dispersion revealed negative anti-Cotton effects at 208 and 228 nm, and a positive effect at 193 nm, indicating an antiparallel double-stranded helix conformation in the aggregates. Encapsulation experiments were carried out with encapsulated FITC labeled PEG2000. Collapse of the vesicles and subsequent release of fluorophores was demonstrated by addition of Triton X-100. Notably, the g.A-PEG vesicles were stable even at high detergent concentrations concentrations, which distroyed lipid membrane completely.

Secondary structure is a crucial factor considering protein function and a very desirable element of diblock copolymers. It is a significant advance towards control of complex biological functions to mimic precise three-dimensional protein folds. A first step to avoid difficulties in structural prediction is the organized self-assembly of small peptides exhibiting specific secondary structure. Fujita et al. [20] used α-aminoisobutyric acid (Aib) containing peptides to obtain α-helical structures of more than 8 amino acids. CD spectra of TFA$^-$ H-(Ala-Aib)$_8$-OBzl$^+$ show characteristic CD

signals for α-helical conformation. The average radius of self-assemblies in water was determined between 30 and 40 nm with a low polydispersity of 0.11, as confirmed by dynamic light scattering and TEM images. It should be mentioned that there is a very delicate balance between hydrophilicity and hydrophobicity. Already low ionic strength or presence of water-soluble dyes caused immediate precipitation of the peptides. Smaller peptides like (TFA$^-$ H-(Ala-Aib)$_8$-OCH$_3$$^+$) did not form molecular assemblies large enough to be detected by DLS, even at high concentrations.

α-Helices and β-sheets can be constituted by consecutive single amino acid sequences. Since it is challenging to synthesize repetitive (especially hydrophobic) sequences exceeding about 10 amino acids by solid phase Fmoc synthesis, larger oligopeptides of this size need to be polymerized by ring-opening reactions. Kukula [17] and Chécot [14] synthesized block copolymers consisting of polybutadiene and polyglutamic acid by combination of anionic and N-carboxyanhydride ring-opening polymerization. Polyglutamic acid is known to form α-helical secondary structure in its uncharged state below pH 4.5 whereas it adopts random coil conformation when negatively charged above its pK. The aggregates' size depends as well on the ratio of polybutadiene to polyglutamic acid; smaller ratios tend to form micelles with hydrodynamic radii of about 16 nm (PBD$_{27}$-PGA$_{64}$) [17] whereas PBD$_{40}$-PGA$_{100}$ [14] diblock copolymers form well defined vesicular morphologies of about 120 nm diameter after direct dissolution in water. Functionality is introduced by deprotonation of glutamic acid. Size and secondary structure is reversibly influenced by changing pH and ion strength.

Vesicles have also been prepared from pure diblock copolypeptides [21-23]. Deming and coworkers [21, 22] demonstrated that purely peptidic species consisting of poly(Nε-2-(2-(2-methoxyethoxy)ethoxy)acetyl-L-lysine-lysine) and poly(L-leucine) [21], as well as poly-L-Lysine and poly(L-leucine)[22] can form micrometer scale vesicles. Most uncharged amphiphilic diblock copolymers within a compositional range of 30 to 60 mol% would be expected to form small spherical or cylindrical micelles in aqueous solution. It is remarkable that the K$_x$L$_y$ copolypeptides deviate from this trend (10 – 40 mol%) probably due to rigid chain conformation and strong interactions between them. The importance of stable helical conformations of either one or both copolymer domains was confirmed by introducing racemic amino acids since none of them formed micrometer scale vesicles.

Short amphiphilic structures entirely constructed of amino acids inspired by lipids were synthetized by von Maltzahn et al. [23]. These structures are 2.5 to 4.7 nm in size and accordingly are denoted "surfactant-like peptides". The hydrophilic head group consists of one or two positively charged amino acids (lysine or histidine); the tail is assembled of 6 hydrophobic residues (valine or leucine). The advantage of such short sized peptides is the possibility to synthesize them by standard Fmoc solid phase synthesis. On the downside, secondary structure can hardly be taken into account due to limited molecular size. Unlike Bellomo's large polymerized α-helical diblocks [21, 22] these peptides' overall structure is hydrophilic enough to be directly dissolved in deionized water. The headgroups were placed alternatively at the C- or the N-terminus which did not lead to significant structural differences. DLS measurements were carried out at pH 4, 7, 9, 12. Two general trends could be observed: Below a peptides pI, discrete nanostructures appeared in solution (hydrodynamic radius = 30-50 respectively 100 – 200 nm), above the pI the structures changed and sizes could not be determined anymore by DLS. Quick-freeze/deep-etch TEM images of V_6K_2 revealed supramolecular organization of nanotubes connected through multiway junctions.

A further step in complexity was achieved by Ye et al. [24]. Even though their system is soluble in water we believe that it is relevant to the topic of peptide self assembly since it represents a further step in introducing complex interactions. Unlike most biological α-helices Ye et al. designed peptides composed as sequential α-helical amphiphiles (Figure 4) and connected two of them each to a bundle connected by a disulfide bridge.
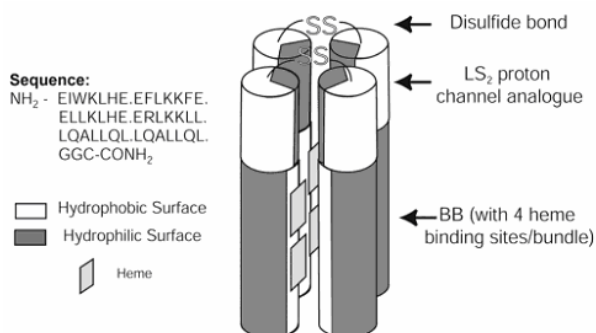

Figure 4 Schematic Illustration of 4-helix bundles[24]

The helices remain amphiphilic over their entire length; polar and apolar regions are supposed to face each other along the helical axis. Histidine 10 and histidine 24 of two opposite helices can coordinate Heme to form two bis-histidyl metalloporphyrin complexes. The absorption of this coordinated porphyrine is shifted to red and hence, by titration, provides evidence for the intended mutual orientation of the helices. These peptide bundles represent an artificially designed structure of higher biomimetic functionality.

Macromolecules like this are at the center of the action in biological processes and their structures represent the key to their function. Since strong advances were made recently in studying self assembled membraneous systems the combined efforts of practical experiments and theoretical considerations gave deepened insight to the physical behavior of amphiphilic block-copolymer self-assembly. As a result, the molecular instrument has broadened from purely lipidic systems to synthetic polymers which outperform lipid membranes in attributes like stability and drug retention, eventually gaining functional diversity by the implementation of peptidic components. Whereas pure lipid and synthetic membranes can be mainly considered as transport vehicles, proteins and peptides have the potential to deploy biological function with the specificity needed to be applied in medicine.

2.3 Gramicidin

This chapter will introduce to the features of the peptide gramicidin with emphasis on primary, secondary, and quaternary structure. We will highlight the aspects that might contribute to the self-assembly processes.

2.3.1 *A Small Peptide With History*

Tyrothricin, an antibacterial extract was first isolated in 1939 by the American microbiologist René Dubos and became the first commercially available antibiotic. Later, it was shown that tyrothricin is a mixture of 80% tyrocidine and 20% gramicidin[25, 26]. It is produced by the soil living bacteria *Bacillus brevis* during its sporulation phase and can be divided into three categories: gramicidin A, B and C, collectively called gramicidin D. The name "gramicidin" originates in the peptides' activity against Gram-positive bacteria[25, 26]. This antibiotic effect arises from the peptides' channel-like structure and the interaction with cell membranes. When

gramicidin is inserted into cell walls, it increases the membrane permeability to monovalent cations. As a result, the ion gradient between the cytosol and the extracellular environment is disturbed and the cell dies. However, gramicidin induces hemolysis at lower concentrations than required for bacteria cell death. It cannot be administered internally and is primarily applied as a topical agent.

Gramicidin has been subject to a large number of biophysical, biochemical, and physiological investigations. It is probably the best understood ion channel to date and has been used as a tool for understanding the process of ion conduction across biological membranes.

2.3.2 *Structural Considerations*

Although gramicidin is a small peptide, it exhibits a surprisingly complex conformational behaviour for several reasons: first, it is a relatively "simple" channel. Usually it is present as a dimer, and each of the monomers it consists of is composed of just 15 amino acids, a feature which makes chemical manipulation of its primary structure facile and examination of "mutants" possible. Second, it forms ion channels with well-defined open and closed states in both black lipid membranes as well as in membrane patches[27]. Third, it binds and conducts monovalent cations[28-30] of different sizes whereas conductance is blocked specifically by divalent cations[31, 32]. On one hand, the regular and stable structure yet small size makes gramicidin suitable for structural studies by techniques like NMR and CD spectroscopy, then again it is a virtually ideal system for molecular dynamic simulations as well as other theoretical studies. Moreover, it crystallizes quite readily and allows studies based on X-ray crystallography.

The primary structure of gramicidin consists of 15 amino acids, alternating in D- and L-configuration:

Formyl-L-X-Gly-L-Ala-D-Leu-L-Ala-D-Val-L-Val-D-Val-L-Trp-D-Leu-L-Y-D-Leu-L-Trp-D-Leu-L-Trp-ethanolamine

where X and Y vary depending on the differing type of gramicidin. Whereas 'X' can be either valin or isoleucine in all species, 'Y' determines which is which; gramicidin A contains tryptophan, B contains phenylalanine and C contains tyrosine.

Most experiments to date were done on the naturally occurring mixture of approximately 80% A, 5% B, and 15% C[33]), which is designated gramicidin D. The sequence of gramicidin has some extraordinary features, which have important implications for its structure and function. First, the peptide is highly hydrophobic throughout the whole length without any charged or hydrophilic side chains present. As a result, gramicidin is never charged, independent from the surrounding pH, which confirms the water-insoluble and hydrophobic property. However, it can be dissolved in a number of organic solvents and inserts readily into the hydrophobic core of phospholipid membranes. This results in dimeric transmembrane structures, which enable the conductance of monovalent cations across the lipid bilayer.

The second important feature of its primary structure is the strictly alternating pattern of L- and D-amino acids throughout its sequence (with the exception of the achiral glycine in position 2). The β-sheet-like folding motif together with the presence of D-amino acids at every second position leads to the channel structure illustrated in Figure 5.
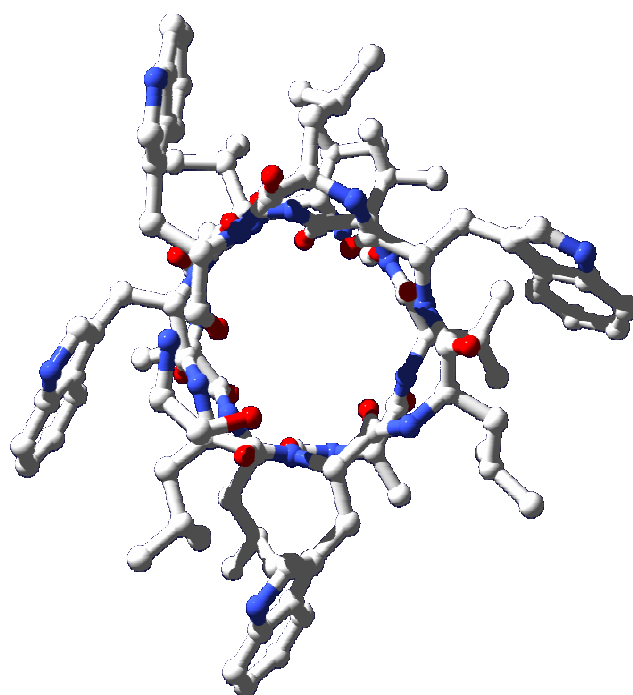

Figure 5 Monomeric gramicidin A helix (1GRM), view along the helical axis. The channel has an inner diameter of about 6.6 Å.

19

Despite the extensive intramolecular network of hydrogen bonds and due to its small size, the molecule is able to adopt a number of different conformations, depending on its environment[34]. This polymorphism is manifested in solution, membranes[30, 34, 35], and in the solid state[36]. Two major "categories" of dimerization were detected: the double helix (dh) and the helical dimer (hd) (Figure 6). The dh type, consists of two polypeptide chains that form a series of intermolecular hydrogen bonds along their entire length. The structure can be described as parallel or antiparallel β-sheet-like motif, which is rolled up to form a helix. This type of structure is often referred to symbolically as a $\pi\pi^{5.6}$ or $\pi\pi^{6.4}$ structure (the superscript indicates the number of residues per turn in each helical monomer). The antiparallel version of the double helix has been designated the "pore" form (Figure 6, left). In a helical dimer, each of the two polypeptide chains forms a similar series of hydrogen bonds along most of its length, but in this type of structure most of them are intramolecular, with the residues at the N-termini of each chain forming several intermolecular hydrogen bonds that join the monomers in an N-terminal to N-terminal antiparallel fashion (Figure 6). This type of structure is called a beta helix and is often referred to symbolically as a $\beta^{6.3}$ structure (again the superscript is the number of residues per turn in the helix) or sometimes as a $\beta\beta^{6.3}$ structure, to emphasize the dimeric nature. It is commonly denoted as the "channel" form (Figure 6, left). Both motifs are composed of β-sheet-like secondary structures, both have their side chains protruding on the outside due to the alternating L- and D-amino acids, and form tube-like structures with the interior of the tubes chemically defined by the relatively hydrophilic polypeptide backbones, whereas the outer surface of the tubes are determined by the hydrophobic side chains. Both types of quaternary structure operate as ion channels in membranes, both have a hydrophobic surface and are able to embed into lipid membranes, and both bind and translocate ions.
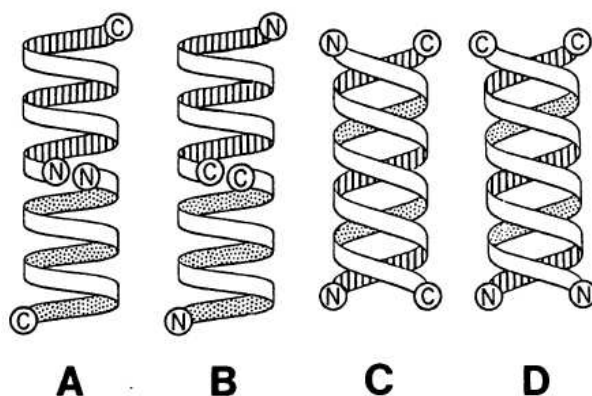
Figure 6 A and B: N to N and C to C helical dimer ($\beta^{6.3}$) conformation of gramicidin. C and D: Antiparallel and parallel double helical ($\pi\pi^n$) conformation.[37]

These two general types of gramicidin structures were originally proposed 1974 by Veatch et al. [38]. and Urry (1972) [39]. Hybrid structures, consisting of partially intertwined helices, may also occur[40] and interconversion via hybrid structures has been suggested[41]. In organic solvents the distribution of conformations, as well as the kinetics of interconversion from one conformation to another, has been shown to be dependent upon the type of solvent, peptide concentration, and temperature[38, 41, 42]. As reflected in the Ramachandran plot (Figure 3) the regions of sterically allowed structures for the polypeptide backbone, are considerably different from those found in all L-polypeptides (Figure 6). Phi and psi angles for β-structures are found in the upper left region (negative Φ, positive Ψ) for the L-amino acids and in the lower right region (positive Φ, negative Ψ) for the D-amino acids. This is the case regardless of whether the parallel or antiparallel motif is present[43, 44].

In a lipid membrane gramicidin can form ion-selective transmembrane channels[45-48]. The channel conformation of the peptide is believed to be an N-terminal to N-terminal, single stranded β-helical dimer[35, 49, 50].The conformation in lipid has well-defined spectral features when measured with circular dichroism (CD)[51] which differ from spectral features found in organic solvents[50] . When gramicidin is added to lysophosphatidylcholine micelles or diacylphosphatidylcholine model membranes from a solution in TFE or dimethyl sulfoxide (DMSO), it directly incorporates in the β-helical configuration[51, 52], whereas upon addition of the peptide as a dry powder or an ethanolic[51, 53] or a methanolic solution in the presence of Cs^+ ions[53], heating appears to be necessary to incorporate gramicidin in its channel configuration. When gramicidin-containing model membranes are prepared via hydration of a mixed lipid/peptide film, subsequent heating results in a change of CD characteristics

toward those indicative of the β-helix while the channel properties become more pronounced[54].

A number of reviews on gramicidin have focused on specific aspects like the role of the primary structure[55], the relationship between pore and channel form[56], its conductance properties[57], physical techniques used to characterize the various structures[58], production of crystals and their characterization[59], molecular dynamics simulations[60], theoretical studies of ion transport[61], interactions with lipids[62], and dynamics and conformational flexibility[63]. Last but not least, details of the structures of the various double helical forms have been elucidated by high resolution X-ray crystallographic and 2D-NMR spectroscopic techniques, which provide important complementary information on structure and dynamics of the peptide in the solid state and in solution.

2.4 Motivation of the Work

Constructing membranes from short peptides is tempting, not only as a feasibility study. Combining the characteristics of a membrane with the functional and structural features of proteins promises supramolecular attributes that are difficult to achieve by lipids or amphiphilic polymers.

However, regarding the lack of publications concerning controlled self-assembly of short peptides, we can conclude that the potential of highly specific intermolecular interactions (section 2.1.2) is often accompanied by a lack of control and thus frequently leads to the formation of gels.

We were looking for peptides that self-assemble to well-defined membranes according to the physical principles responsible for the process of protein folding. We found the desired properties in the structure of gramicidin, which acts as the essential hydrophobic constituent of a membrane forming peptide amphiphile. Studying the structural characteristics of our system revealed complex behaviour of self-assembly.

3 Results

3.1 Characterization of Mass and Purity

Table I shows the synthesized peptides. For a detailed characterization by mass spectroscopy and analytical HPLC of the purified products, see Annex 7.2.1.

Table 6: Synthesized peptides

Name	Structure
gA-K_2	H-K_2-L-G-A-DL-A-DV-V-DV-W-DL-W-DL-W-DL-W-NH_2
gA-K_4	H-K-G-K_3-L-G-A-DL-A-DV-V-DV-W-DL-W-DL-W-DL-W-NH_2
gA-K_6	H-K_3-G-K_3-L-G-A-DL-A-DV-V-DV-W-DL-W-DL-W-DL-W-NH_2
gA-K_8	H-K_2-G-K_3-G-K_3-L-G-A-DL-A-DV-V-DV-W-DL-W-DL-W-DL-W-NH_2
gA-K_{10}	H-K-G-K_3-G-K_3-G-K_3-L-G-A-DL-A-DV-V-DV-W-DL-W-DL-W-DL-W-NH_2
Trunk-K_1	H-K_1-W-DL-W-DL-W-DL-W-NH_2
Trunk-K_2	H-K_2-W-DL-W-DL-W-DL-W-NH_2
Trunk-K_3	H-K_3-W-DL-W-DL-W-DL-W-NH_2
Trunk-K_4	H-K_4-W-DL-W-DL-W-DL-W-NH_2

3.2 Circular Dichroism

3.2.1 The Library

Even though circular dichroism measurements are very sensitive to small changes in the conformation of a chiral molecule, it is difficult to deduce quantitative structural information from CD spectra in the absence of reference data. In the case of wildtype (wt)-gramicidin, circular dichroism is a common technique to deduce the quaternary structure, which, in turn, affects the secondary structure of the peptide. Thus, gaining information about the secondary structure of gramicidin means gaining information about its state of dimerization. In addition, CD provides information about thermal stability, reversibility of unfolding and structural dependence on pH variation and solvent history.

As described in section 2.3.2, gramicidin can adapt two distinctly different states of dimerization that were isolated and described earlier [38, 64, 65]. Accordingly, we distinguish between an intertwined double-stranded helix (dh) initially proposed by Veatch and Blout[38] and a head-to-head single-stranded helix (hd) proposed by

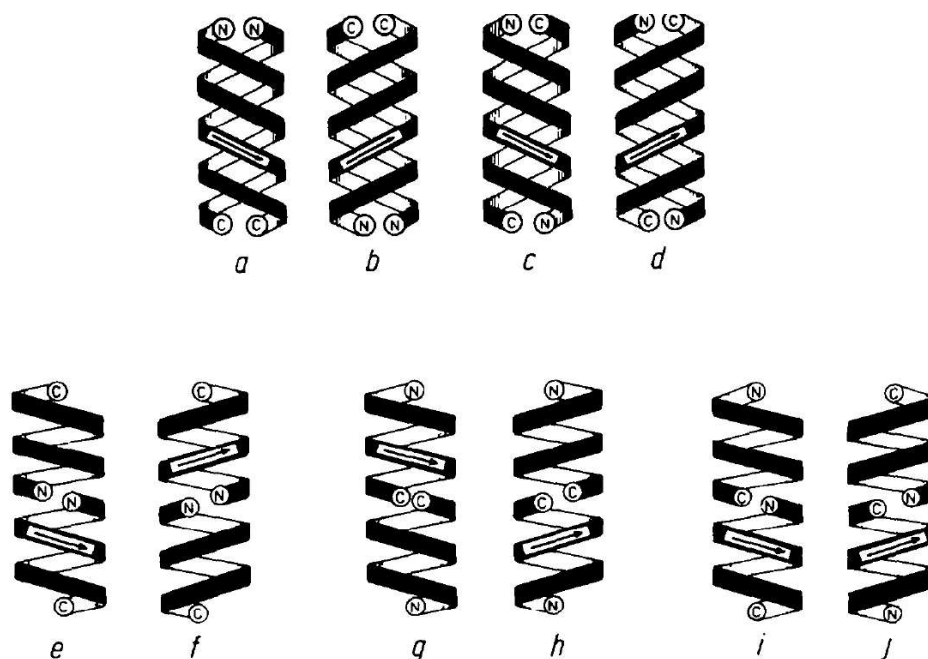Urry.[49]. Each of these can be varied in handedness and relative orientation of the monomers (Figure 7).

Figure 7 Possible quaternary structure of wt-gramicidin:prallel (a, b) and antiparallel (c, d) double helices of varying handedness. E to j shows helical dimers with varying relative orientation and handedness.**[66]**

There is general agreement in literature that the preferred dimerization state of gramicidin depends on the polarity of the environment and its solvent history. Inserting gramicidin into lipid membranes usually causes the peptide to adopt hd conformation, which is assumed to represent the dimerization state of lower energy. However, in organic solvents gramicidin usually adopts double helical conformation: in dioxane, a left-handed antiparallel double helix structure[67] is predominant, while in a solution of methanol/chloroform and CsCl a right-handed antiparallel double helix[68] was found. In ethanol, gramicidin is present in the form of four interconverting double helices: two left-handed parallel, one left-handed antiparallel, and one right-handed parallel[69]. X-ray diffraction studies on gramicidin A crystallized from a CsCl methanol solution[38] and from a benzene/ethanol azeotrope mixture[49] show that these crystal structures are also of the double-helix type.

The solvent dependence of gramicidin quaternary structure is summarized in Table 7. In conclusion, differing structural states of gramicidin measured as a response to differing solvents provides comparative information about the system.

Table 7: Structural characteristics of various forms of wild type gramicidin

Solvent:salt	Technique	Designation	dh/hd	Hand	A/P	R/t	Length	Ref
Ethanol/benzene	NMR	cp	dh	l	A	5.6	36	[67]
Dioxane	NMR	—	dh	r	P	5.7	27	[70]
Ethanol	X-ray	cp	dh	l	A	5.6	35	[71]
Methanol:CsCl	X-ray	op	dh	l	A	6.4	26	[72]
Methanol/CDCl$_3$:CsCl	NMR	op	dh	r	A	7.2	27	[73]
Methanol:KSCN	X-ray	pp	dh	l	A	6.4	26	[44]
Methanol:CaCl$_2$	NMR	bp	dh	l	P	5.7	30	[43]
SDS micelles	NMR	oc	hd	r	A	6.3	24	[74]
DMPC bilayers ss	NMR	oc	hd	r	A	6.5	25	[75]

Abbreviations: cp, closed pore; bp, blocked pore; op, open pore; pp, partially open pore; oc, open channel; dh, double helix (number inparenthesis refers to species as defined in[38], hd, helical dimer; l, left; r, right; A, antiparallel; P, parallel; ssNMR, solid state NMR.

Since the structure of gramicidin has been explored for over 50 years, there is a wealth of CD reference data present in literature. The data gives insight to the characteristics of helical secondary structure and the relation to its state of dimerization. The far-UV spectra of wt-gramicidin in all its different dimerization forms[66] distinctly differ from secondary structure motifs frequently appearing in proteins like α-helices, β-sheets and random coils (Figure 8) however, due to multiple structurally closely related dimerization forms and mixtures thereof there is often no straightforward interpretation of CD spectra (Figure 9) and they are rather comparative in nature.
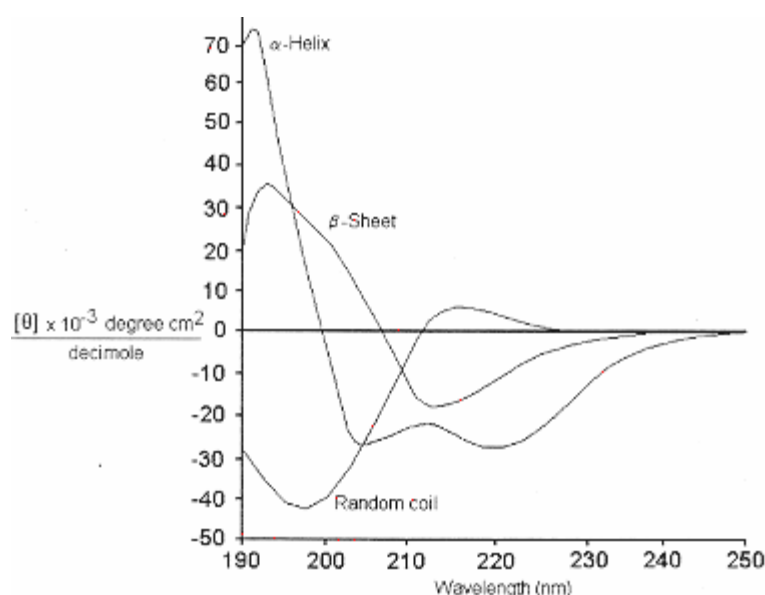

Figure 8 Reference CD spectra of the most common secondary structure motifs – α-helix, β-sheet and random coil.

In addition, it should be kept in mind that the molecules synthesized in this work are not identical to the wildtype since neither the formyl- nor the ethanolamine-modification is part of our synthetic structures. Moreover, the attached sequence of oligo-lysine might influence the helical structure as well.

Figure 9 shows the concentration-corrected CD spectra of gA-K$_x$ (x = 2, 4, 6, 8 and 10) (see Table 6 for a detailed structural description).
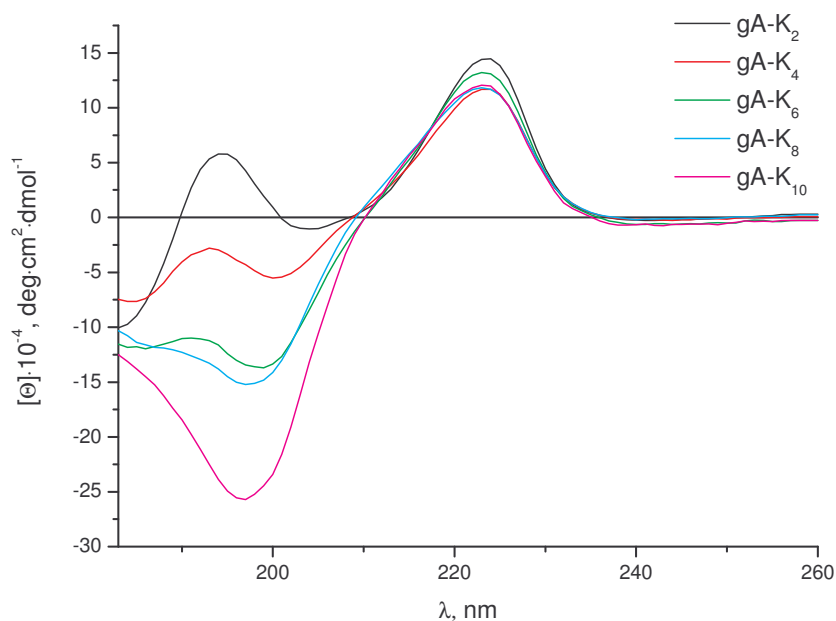

Figure 9 CD spectra of all synthesized gA-peptides with varying lengths of oligo-lysine. The measurements were carried out in water.

Charged oligo-lysine peptides adopt random coil secondary structure, which corresponds to the increasingly negative ellipticities between 180 and 210 nm (for a set of reference spectra see Figure 8). Systematic variation of the molar ellipticity in this wavelength range stands out and is appointed to the increasingly negative contribution of random coil structure with increasing numbers of lysine residues. Random coils do not contribute much to the CD signal at wavelengths higher than 210 nm and consequently, the range in between 210 and 260 nm can be assigned almost entirely to the 15 amino acids of gramicidin. Consequently, the intensity as well as the peak position at 223 nm is nearly unaltered as the lysine chain length changes and we can conclude that the extent of helical secondary structure of

gramicidin is not affected by the length, and probably not even by the presence of oligo-lysine.

In addition, the systematic variation of oligo-lysine in length allows for extrapolation to the unadulterated CD spectrum of the gramicidin helix in the wavelength range between 180 to 210 nm without the contribution of a random coil. Emanating from this, the far-UV spectrum exhibits two distinct maxima at 223 nm and 196 nm and can be compared to CD studies performed earlier on unmodified wt-gramicidin. Figure 11[38] displays far UV CD spectra of varying gramicidin dimers. The dashed spectrum in the left diagram most closely corresponds to our data.

According to Wallace[76], it should be interpreted as a right handed parallel double helix, however, it should be emphasized that Veatch et al.[38] also conceded the possibility of a helical dimer. One must emphasize that a parallel double helix is very unlikely to occur in our samples since the construction of a membrane would demand two parallel double helices, assembled to a head-to-head dimer (Figure 10).
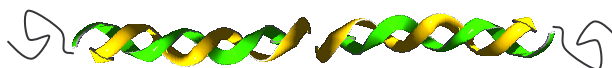

Figure 10 Hypothetical structure describing a head-to-head dimer of two double helices (based on 1ALZ).

However, the occurrence of a structure like this is unlikely since no Gramicidin tetramers have been observed earlier (Figure 10). No reference could be found showing CD spectra of right-handed *antiparallel* double helices even though there is evidence of their occurrence by 2D-NMR studies[66, 77].

In addition to the uncertainty arising from the qualitative nature of CD experiments, we point out that the wavelengths of both maxima in our spectra are blue-shifted by roughly 5 to 10 nm compared to corresponding wt-gramicidin spectra, which might be appointed to the variation in primary structure and the peptide self-assembly to membranes or micelles.
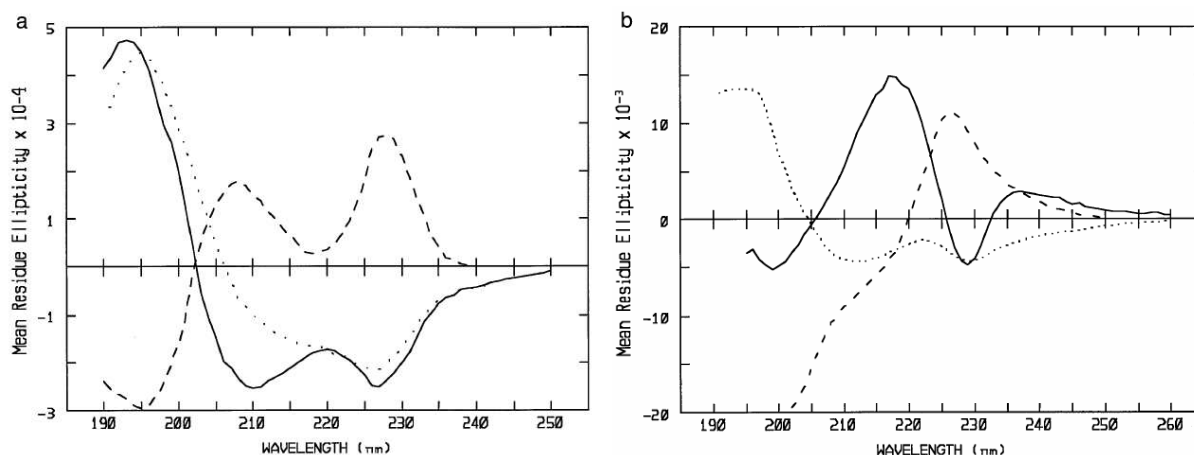
Figure 11 Reference CD data of gramicidin in its double helical (a) form and helical dimer (b) appearances[78]. a: (—) describes the left-handed parallel double helical form, (···) corresponds to the left-handed antiparallel double helical form and (---) is the right-handed parallel dh form. b: (···) is the ion-free hd form and (---) the Cs^+ containing hd form. (—) is the double helical form in DMPC vesicles.

Equivalent measurements were performed on Trunk structures with 1, 2, 3 and 4 lysines attached (Figure 12). Lysine residues lead to decreased values of molar ellipticity in between 185 and around 210 nm. Again, increasing the lysine chain length does not lead to a shift in intensity or wavelength of the maximum. The peak position at 223 nm is identical to the spectra of gA-K_x.
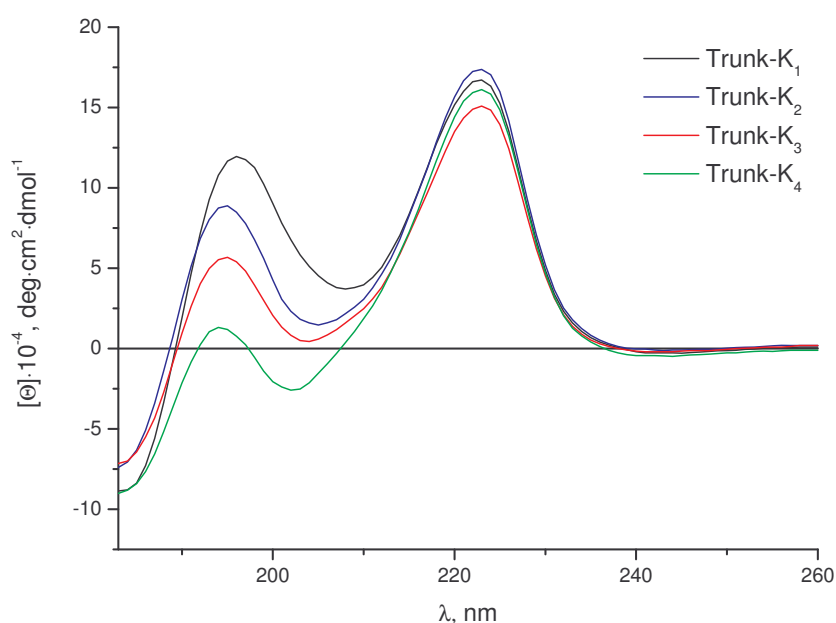

Figure 12 CD spectra of all synthesized Trunk-peptides with varying lengths of oligo-lysine, carried out in water.

28

Trunk-K $_1$ must be close to the secondary structure of "pure" Trunk peptides and exhibits two maxima: one at 196 and 223 nm and, comparing it to gA-K$_2$ suggests identical secondary structure in both peptide families. Since the secondary structure is determined by the state of dimerization, we conclude identical dimerization behaviour in case of gA and Trunk derivatives. Contrary to gramicidin, most small peptides depend upon disulfide linkages or prolines to provide stability for a well-defined three-dimensional conformation. The stability of our peptides is even more remarkable when the absence of long-range structural constraints is considered; there is only one single helical domain and the peptide does not fold back on itself. Consequently, there is no tertiary structure, but only a mixture of primary, secondary, and quaternary structures. The quaternary structural aspect of this conformation may add considerably to its stability, since a stable monomeric and helical conformation of gramicidin has not been observed[79].

3.2.2 *Quantitative Comparison of Helicity in Trunk and gA*

The intensity of CD spectra linearly depends on the concentration (or occurrence) of secondary structure in a sample. Correcting the measured ellipticity for sample concentration $[\theta]$ and additionally to the number of amino acid residues $[\theta]_{MRW}$ provides information about the averaged amount of a secondary structure motif within one molecule or, in other words, the helicity of our peptides.

By approximation, we can assign the wavelength range in between 200 and 260 nm to the sequence of alternating D- and L-amino acids and thus, it is possible to compare gA to the Trunk in terms of helical abundance. Longer peptides have higher probability to build structural elements like loops or turns to support well-defined 3-dimensional structure. Gramcidin, together with S-peptide (an α-helical part of RNAse A) is one of the shortest peptides known to exhibit distinct secondary structure. The relation of sequence to structure is extraordinary but becomes plausible by consideration of the stabilizing effect of dimerization. It stands to reason to compare the mean molar residue ellipticity $[\theta]_{MRW}$ of a Trunk with a gA peptide (Figure 13).
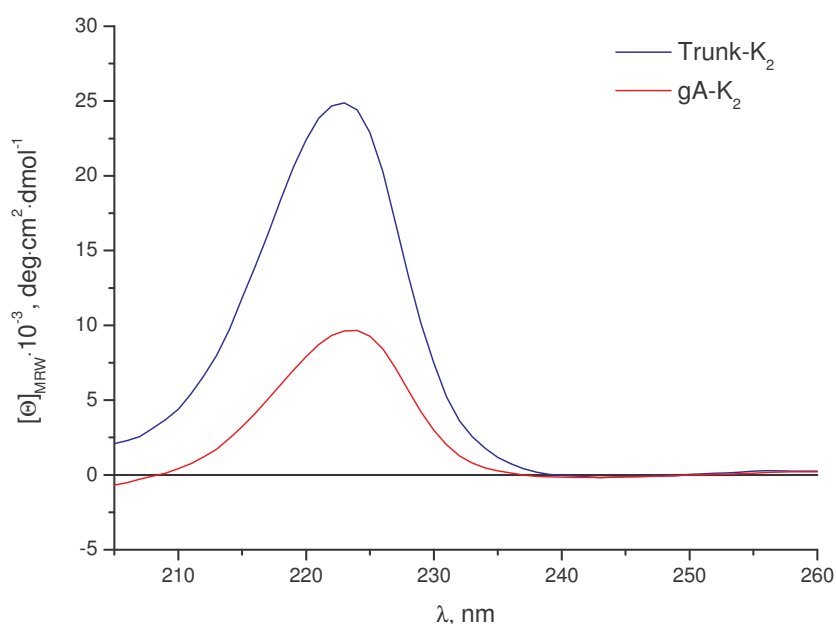
Figure 13 Comparison of Trunk and gA CD spectra.

The spectra in this diagram are tempting to deduce that reducing the wt-gA sequence to its last seven amino acids leads to a promotion of helicity in the shortened structure. However, since gramicidin is able to adopt several forms of dimerization, it is possible that a different structural motif contributes to the spectrum and weakens the signal at 223 nm. This, in turn, is unlikely since the peak position does not change, which could be only due to a spectrum close to 0 ellipticity between 210 and 260 nm (corresponds to a random coil) or to a mirror image of the obtained spectrum, caused by an identical helical motif with opposite handedness.

Considering the above idea and assuming an equililbrium between a helical conformation and a random coil state (lower ellipticity at 223 nm) in both species, it makes sense to assume that both structures, Trunk and gA, are in dynamic equilibrium between folded and unfolded state. In addition, it is very likely that both structures exhibit the same secondary structure and state of dimerization. It is known from small peptides that only a part of the molecules are in the folded state at room temperature (S-Peptide: 10 to 50 %) yet it is surprising that a sequence fragment of gramicidin (Trunk) has a higher equilibrium constant of folding than gA by the factor of about 2.5.

3.2.3 *Thermal Stability and Reversibility of Unfolding*

The thermal stability can be assessed using CD by following changes in the spectrum with varying temperature. It is remarkable that secondary structure of gA and Trunk is detectable in water, organic solvents (EtOH, ACN, DMF) and even 8M urea does not fully destroy it. However, increasing the temperature unfolds the helical structure.
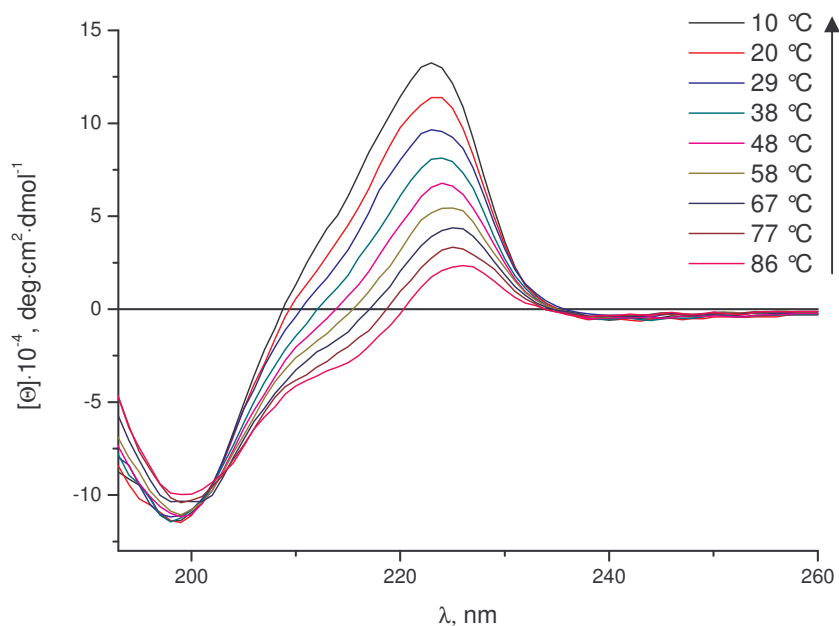

Figure 14 CD spectra of gA-K$_8$ taken at every 10 °C upon cooling down from 86 °C.

Figure 14 shows CD-spectra at temperatures intervals of about 10 °C in between 10 and 86 °C starting at the highest temperature. Lowering the temperature to 10 °C causes an increase of secondary structure concentration by the factor of 7.6 and since $\dfrac{\partial \theta}{\partial T}$ can be approximated linearly (Figure 16) we can roughly assume a loss of 10 % of the initially present secondary structure per 10 ° in water.

The spectra displayed in Figure 15 demonstrate the ability of gramicidin to rebuild helical secondary structure once it was thermally unfolded. The behaviour becomes even more obvious in Figure 15 where samples of gA-K$_8$ and Trunk-K$_3$ were measured three times; initially at 20 °C, at 80 °C and then after cooling down to 20 °C again. The process of heating and cooling took approximately 30 min and in summary it can be said that the peptides refold to their initial secondary structure with

very little loss in secondary structure. Additionally, it can be concluded that the lysine chain length does not influence the ability to renature.
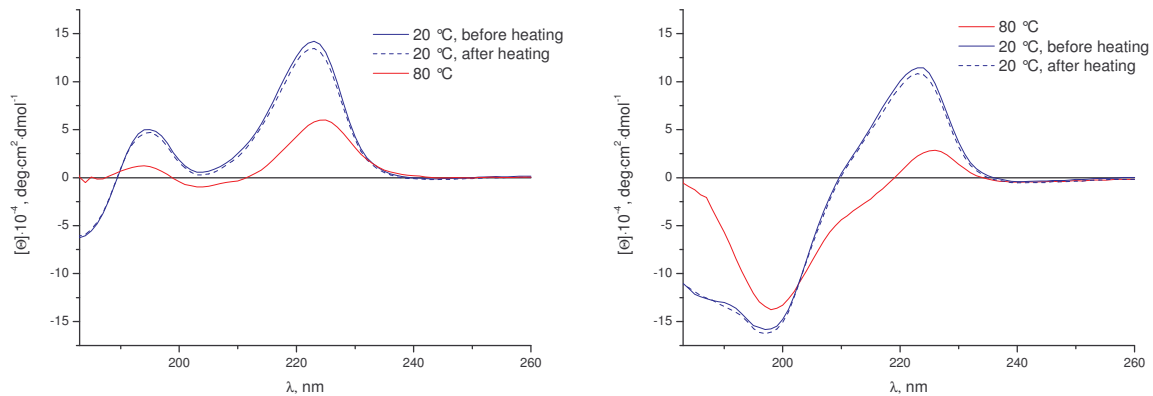

Figure 15 Heat induced denaturation of gA-K$_8$. The initial measurement was taken at 20 °C, then the samples were heated to 80 °C and cooled down again to the initial temperature.

Many proteins aggregate quickly after they are unfolded, making the process irreversible. As a control, the reversibility of the unfolding reaction was affirmed by cooling the sample and then heating it up again to reproduce the process of unfolding.

In Figure 16 the temperature dependent variation of $[\theta]_{MRW}$ was observed at 223 nm. As described in section 3.2.2, $[\theta]_{MRW}$ was calculated considering 15 helical residues for gA-K$_8$ and 7 in the case of Trunk-K$_3$.

The width and shape of $[\theta]_{MRW}(T)$ indicates quantitatively the cooperativity of the unfolding reaction. Since there is no apparent melting temperature (inflection point) in the measured interval, it is not possible to obtain the enthalpy of unfolding. A highly cooperative unfolding reaction (explicit sigmoidal shape) indicates that the protein existed initially as a compact, well folded structure. By contrast, a very gradual, non-cooperative melting reaction signifies that the protein existed initially as a very flexible, partially unfolded protein or as a heterogeneous population of folded structures. Since our peptides do not exhibit tertiary structure, we can conclude that the defined helical arrangement is in thermodynamic equilibrium with an unstructured conformation. It should be emphasized that the thermodynamic parameters of this equilibrium cannot be quantitated due to the uncooperative denaturation behaviour. Working at room temperature therefore includes an unknown fraction of unfolded

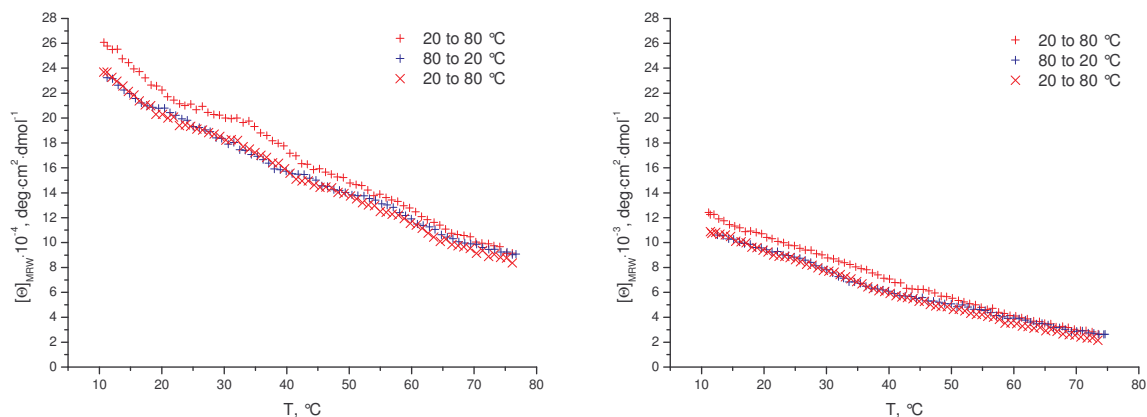peptide since lowering the temperature of the samples below 20 ℃ consistently increases θ at 223 nm (see Figure 14).

Figure 16 Temperature dependent unfolding and renaturation of Trunk-K$_3$ (left) and gA-K$_8$ (right).

However, the thermal denaturation, as well as renaturation curves of gA and Trunk demonstrate the ability of all peptides to reversibly unfold and it can be said that the solubility of the molecules is not affected by denaturation, since unfolding of our peptides is not expected to alter the contact area of hydrophobic residues to the solvent.

3.2.4   *Solvent Dependence*

We measured CD in ethanol, trifluoroethanol (TFE) and aqueous solution at neutral pH. Comparing CD-spectra of all molecules reveals that the helical secondary structure (223 nm) is always most intense when the samples were in water. This becomes most evident in the case of Trunk-K$_1$ (Figure 17) where there is just small influence of the lysine secondary structure. Ethanol seems to interfere most with the formation of the helix since comparing θ at 223 nm reveals about 12 % helicity of Trunk-K$_1$ in EtOH compared to H$_2$O.
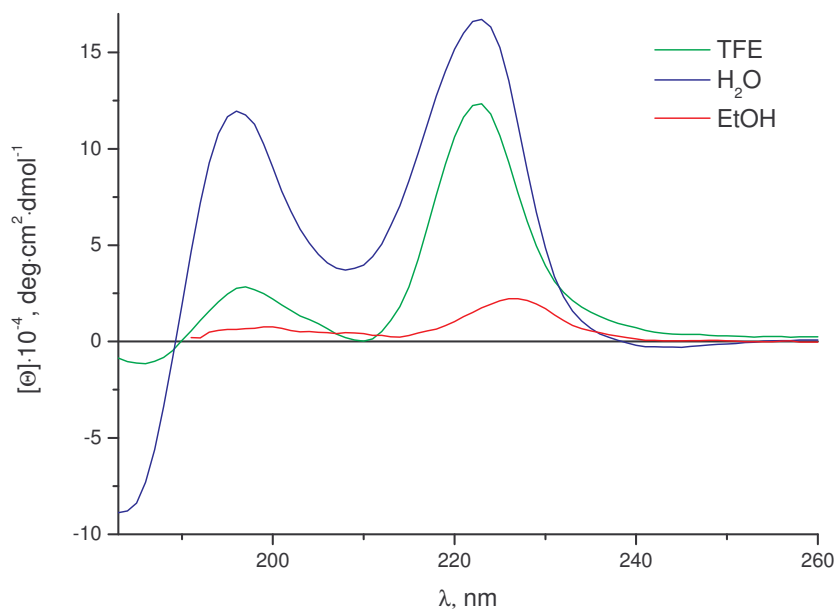
Figure 17 Mean molar ellipticities of Trunk-K_1 in H_2O, TFE and ethanol.

However, TFE and, in a lower extent, EtOH promote the α-helical conformation of oligo-lysine which exhibits more negative ellipticity than a random coil between 205 and 250 nm (compare to Figure 8). Thus, the peak at 223 nm will be lowered due to the formation of an α-helix. gA-K_{10} in Figure 18 demonstrates the intersection of ellipticities in the spectra of water and TFE at about 205 nm which is typical for the conformational change from a random coil to an α-helix.

Wt-Gramcidin can adopt different quaternary structures (see section 2.3) in organic solvents of varying polarity and in lipid membranes after cosolubilization in organic solvents (Table 7). We also need to consider that the secondary structure of gA can depend on its solvent history[34, 65, 77, 79-82]. However, we could not observe adaption of different dimer forms in solvents of varying polarity.
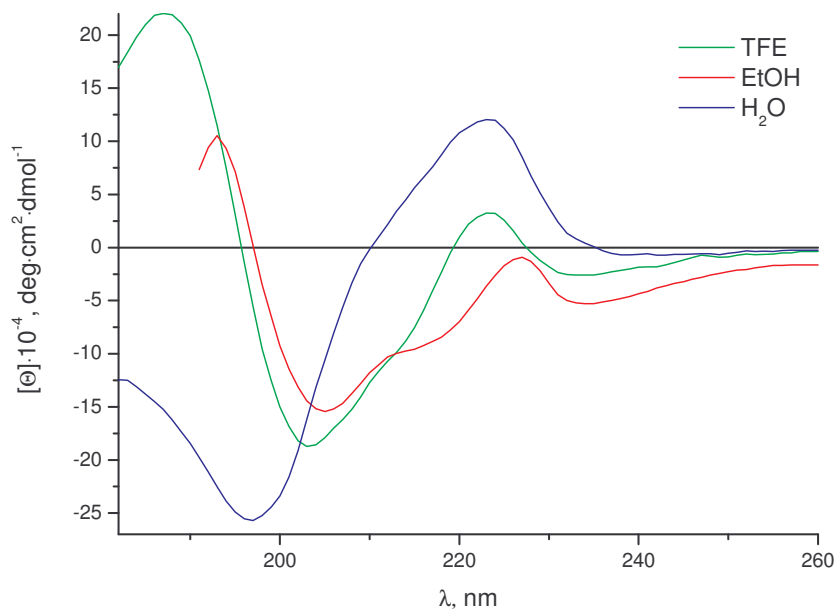
Figure 18 Mean molar ellipticities of gA-K$_{10}$ in H$_2$O, TFE and Ethanol. Oligo-lysine adopts α-helical conformation in EtOH and TFE.

3.2.5 *pH Dependence*

We do not present pH dependent CD data since most of the samples precipitate in pH > 10 and disturb the measurement due to scattering effects. In addition, it is not possible to measure below 205 nm at this pH since the absorption of NaOH is too high even with a cuvette path length of 0.1 cm. Measuring below 200 nm would be necessary to observe the formation of an α-helix which exhibits strongly positive ellipticities at around 190 nm.

3.3 Antimicrobial Effect

The bactericidal effect of wt-gramicidin might be lost due to the chemical modification with oligo-lysine. We applied gA-K$_6$ and commercially available gramicidin D to *Staphylococcus aureus* wild type (SA113 wt) and its mutant *Staphylococcus aureus* ΔdltA (SA113 *ΔdltA*) and compared to their antibiotic impact. The mutant SA113 *ΔdltA* is especially sensitive to cationic peptides like poly-lysine.

Table 8: Antibacterial Properties of gramicidin D and gA-K$_6$

Peptide	MIC* (μg/mL) SA113 wt	MIC* (μg/mL) SA113 ΔdltA	MBC** (μg/mL) SA113 wt	MBC** (μg/mL) SA113 ΔdltA
gramicidin D	12.50	6.25	>50.00	50.00
gA-K$_6$	12.50	12.50	>50.00	50.00

* Minimal inhibition concentration
** Minimal bactericidal concentration

The results in Table 8 show that the antibacterial effect of gA-K$_6$ is comparable to wt-gramicidin D. The MBC reveals that neither gA-K$_6$ nor gramicidin D fully distroy all wt bacteria at the highest measured concentration but both distroy completely the ion sensitive mutant SA113 ΔdltA. The antimicrobial effect of gramicidin is caused by the ability of the molecule to guide monovalent cations through lipid membranes. However, it is not known to date which dimerization form (hd or dh) is biologically active and therefore, antimicrobial assays do not contribute to the discussion about the dimerization structure of our samples.

3.4 Transmission Electron Microscopy

Since our peptides build supramolecular assemblies in the size range of around 200 nm, we applied gA-K$_8$ from an aqeous solution to a transition electron microscope. The pictures reveal spherical structure (Figure 19 andFigure 20) with a size range of around 200 nm. However, structural interpretation from TEM pictures always need to be taken with a grain of salt since the samples are measured in vacuum which may alter the shape and polydispersity of the objects. However, further evidence for the vesicular nature of the particles is given with Figure 20, which can be interpreted as a collapsed vesicle membrane.
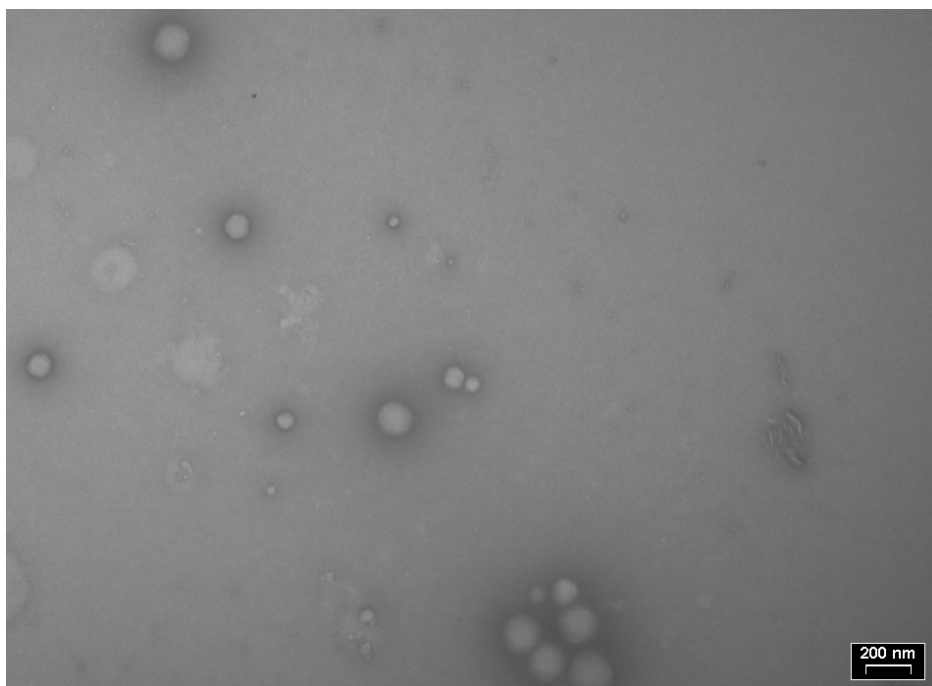
Figure 19 Uranylactetat stained TEM picture of gA-K$_8$ sample.

The grainy background of Figure 20 at higher magnificiation can be interpreted in terms of micellar structures and is discussed further by dynamic light scattering data obtained in section 3.7.
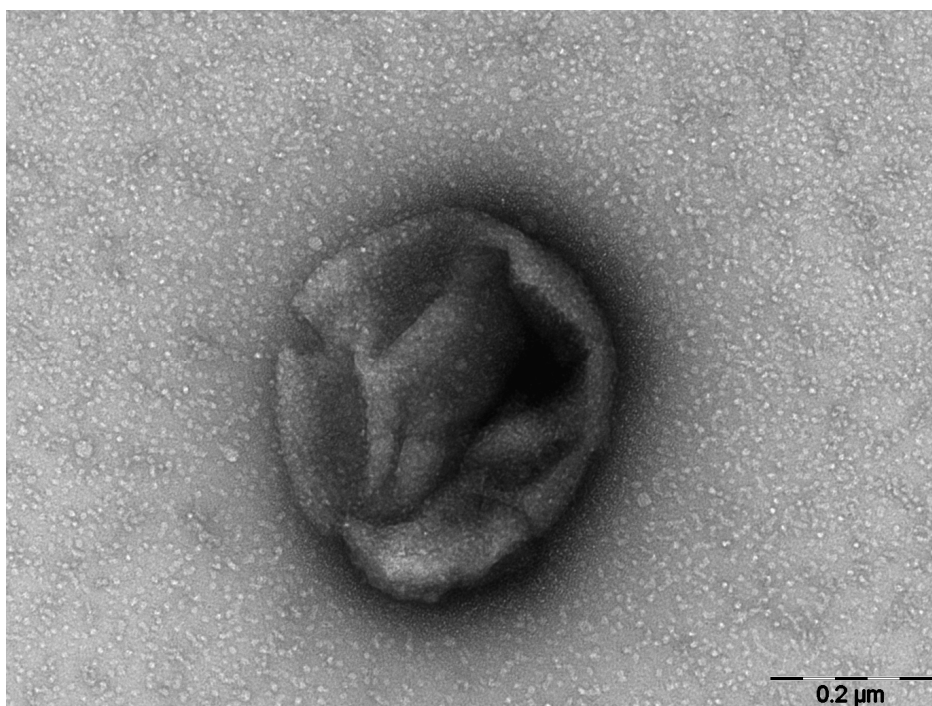
Figure 20 A collapsed vesicle and evidence for micelles (stained gA-K$_8$)

3.5   Scanning Electron Microscopy

Scanning electron microscopy pictures were taken of gA-K_8 and Trunk-K_3. Representative examples are shown in Figure 21 and Figure 22 Since the samples were lyophilized from an aqeous solution, the same constraints like at the TEM measurement need to be considered. The absence of water might influence the structural properties of the sample, which manifested in an altered size and size distribution. Nevertheless, both SEM pictures amend the conclusions from the TEM measurements and reveal the spherical shape of the assemblies. We propose that the holes in the structures arise from lyophilization, where encapsulated water expands due to the vacuum and hence breaks the surrounding membrane.The rocess leads to the observed "egg shells".

Figure 21 SEM of gA-K_8 sputtered with gold

However, it should be mentioned that the broken vesicular structures might also be due to a slow freezing process of water.
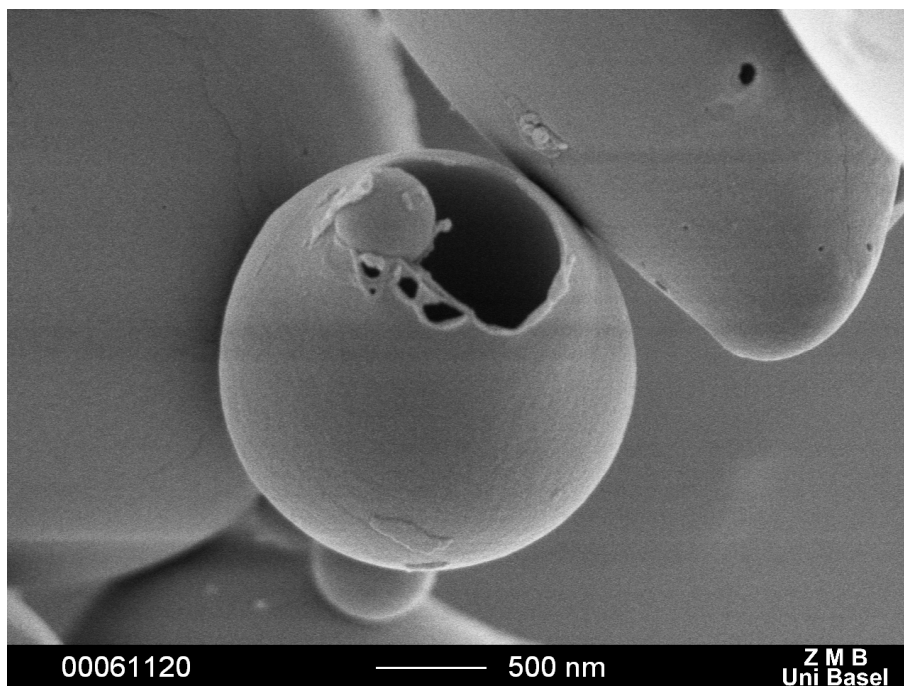
Figure 22 SEM of gA-K$_8$ sputtered with platinum.
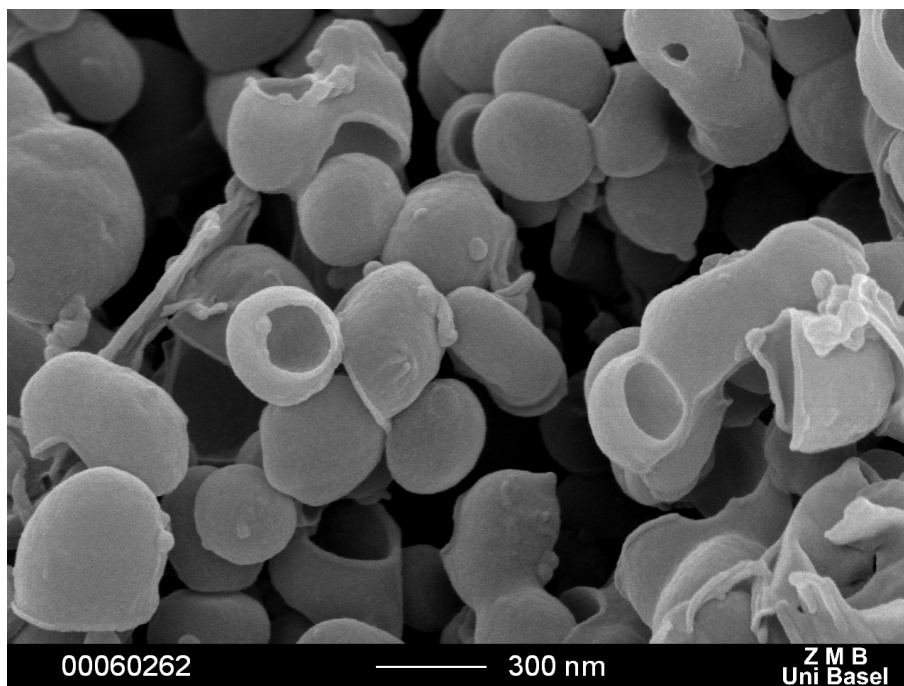
3.6 Atomic Force Microscopy

Since it is not possible to extrude the peptide samples with a lipex gas pressure extruder (up to 70 bar) it is assumed that the vesicle membrane is very rigid and thus, might maintain its shape at the solid-air interface. The assumption is confirmed in Figure 23 where the vesicles did not collapse even though the outer hydration shell was removed. The size range and polydispersity can be compared to the samples measured by TEM (section 3.4) and dynamic light scattering (section 3.7.2). and are within the same size range. The measurement reveals rather monodiperse spheres on a negatively charged mica surface, which might be the reason for the adhesive force between the surface and the spheres. Residual water might be responsible for the particle clusters due to the capillary effect.

It is also worth mentioning that there is only minor deformation of the vesicles since diameter and thickness of the objects largely correspond to each other.
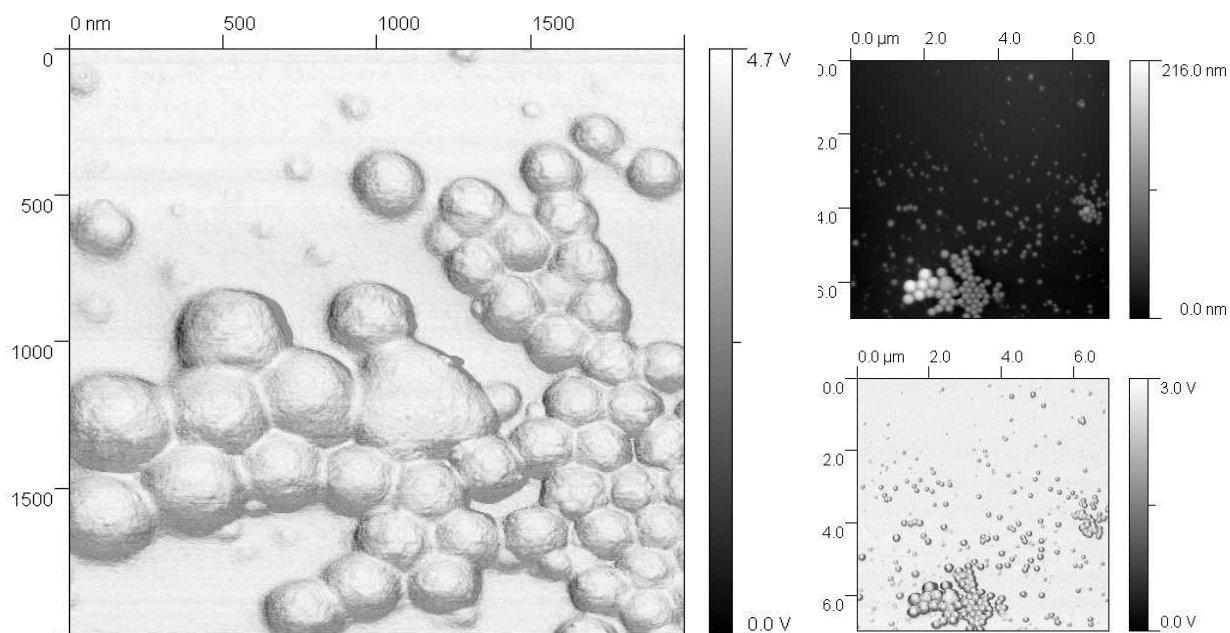
Figure 23 AFM of gA-K$_8$ at the solid-air-interface.

3.7 Light Scattering

Light Scattering (LS) was applied to analyse the size distribution of the peptide assemblies. In contrast to microscopy techniques, LS provides statistically significant information about the size distribution of objects in solution.

3.7.1 *Angular Dependent Dynamic Light Sacttering*

Table 4 shows a cumulant fit analysis of a Trunk-K$_3$ sample shortly after dialysis (left column) and after 5 days of annealing at 70 °C (right column). Initially, the particle size distribution of the sample is broad and cannot be fitted properly to one population by means of a cumulant or contin analysis.

Table 4: Cumulant Fit Data of Trunk-K_3

Angle	1st Day		5th Day	
	2nd order r_H	PdI	2nd order r_H	PdI
30	274.23	0.427	201.97	0.0554
40	265.76	0.454	191.21	0.107
50	215.72	0.427	184.41	0.0648
60	197.44	0.344	175.02	0.0565
70	183.84	0.303	163.26	0.095
80	180.65	0.36	151.30	0.104
90	179.37	0.396	147.74	0.156
100	172.81	0.413	143.07	0.135
110	187.48	0.451	142.7	0.178
120	192.93	0.469	147.50	0.209
130	184.11	0.452	154.9	0.261
140	193.67	0.461	166.87	0.343
150	146.84	0.427	185.89	0.42

However, when exposing the sample to a higher temperature, the size distribution changes; the second column of Table 4 shows cumulant fit data after 5 days of annealing at 70 °C. The fitted polydispersity is below 0.2 at angles below 120° and below 90°, the highest occurring PdI is even below 0.1, which is unusual for the population in the size range of around 400 nm in diameter. Yet, the size distribution in the sample at angles >120° remains polydisperse. Considering the explicit trend of the correlation function towards shorter lag times at high angles (Figure 24) and comparing it to the regular and grainy background pattern at the 10 nm size range in the TEM pictures, we hypothesize a second population of smaller structures, possibly micelles (see also section 3.4)
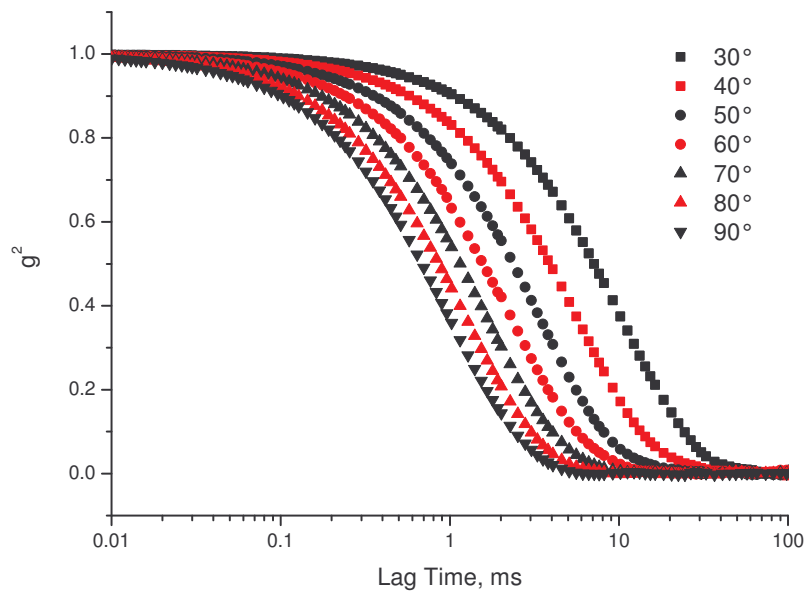
Figure 24 Correlation functions of Trunk-K_3 from 30 to 90°, measured after 5 days of annealing at 70 °C.

However, due to the very monodisperse size distribution of large objects measured at small angles, we conclude that a linear fit of 1/r vs. q2 (Figure 25) is useful in the range between 30° and 90° where mainly large objects contribute and the influence of small objects are disregarded at (θ < 100°). Extrapolating the linear fit to $q^2 = 0$ reveals a hydrodynamic radius of 219 nm.
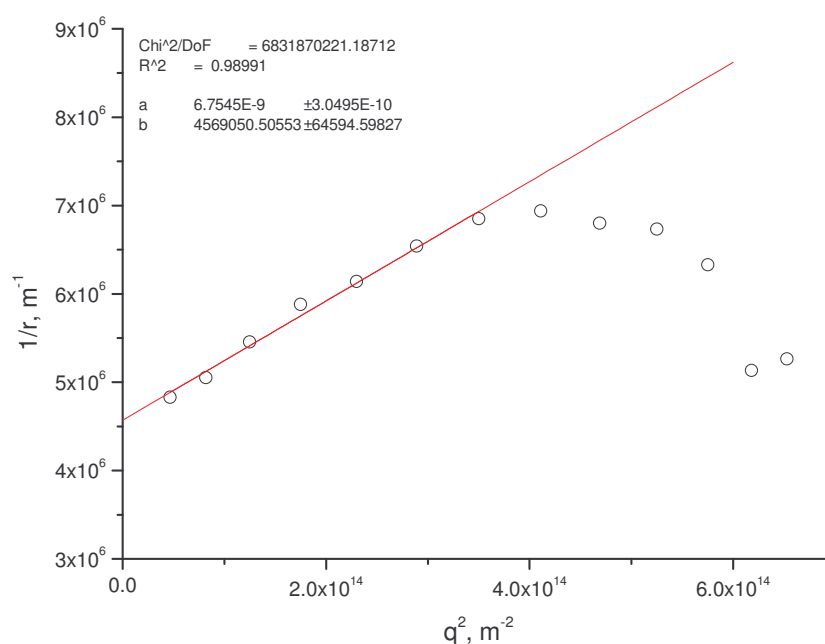
Figure 25 R_H calculated by the 2nd order cumulant fit on angles between 30° and 150°. The values in between 30° and 90° were fitted linearly and extrapolated to 0.

The annealing experiment (Table 4) combined with light scattering measurements shows that the procedure of sample preparation matters in terms of size distribution and polydispersity of the samples. A very monodisperse population of particles with an average hydrodynamic diameter of 440 nm emerges after exposing the peptides to higher temperature. However, smaller objects remain unaffected and contribute to the light scattering measurements at high angles. To find the concentration distribution of large and small objects in our samples, we applied it to a Centricon tube with a cutoff od 100 kDa and compared the peptide concentration before and after filtering. We excluded an extrusion effect arising from the Centricon pores by multiple centrifugation runs and comparison of the resulting concentrations. A cutoff of 100 kDa is sufficient to let single molecules and micelles pass whereas objects with a diameter of 440 nm are certainly retained. Immediately after dialysis, the fraction of peptides that passed the filter amounted for 98 % whereas 50 % were retained after 5 days of annealing.

3.7.2 *pH Dependent Aggregation*

Variation of macromolecular structure can be observed by a change of pH; the hydrophilic lysine block attached to each of our peptides induces amphiphilicity to the peptides in the charged state below its pK of 10. These hydrophilic lysine residues allow the peptides' favorable interaction with water and thus, play an important role concerning the self-assembly of the membrane. At the same time, lysine represents a molecular switch that, above pH 10, becomes deprotonated and thus, results in a decrease of the molecular hydrophilicity.

Figure 26 Dialysis tube with gA-K$_6$ at pH 7 before addition of NaOH (left), precipitated at pH 12 (middle) and at pH 7, after dialysis of the precipitate against water (right).

Figure 26 shows pictures of the peptide samples in the dialysis tube. The opalescent appearance is evident at pH 7 before and after exposure to pH 12 (left and right picture). The picture in the middle shows the aggregated protein at pH 12.

Figure 27 andFigure 28 show dynamic light scattering data at 90° before and after addition of NaOH to a pH of 12. The inset diagram shows the contin fit which exhibits two size population with hydrodynamic radii of 10 about 130 nm. Both are present before and after base addition. The size distribution given by the polydispersity index (PdI) did not change significantly comparing the colloidal state before and after basification.
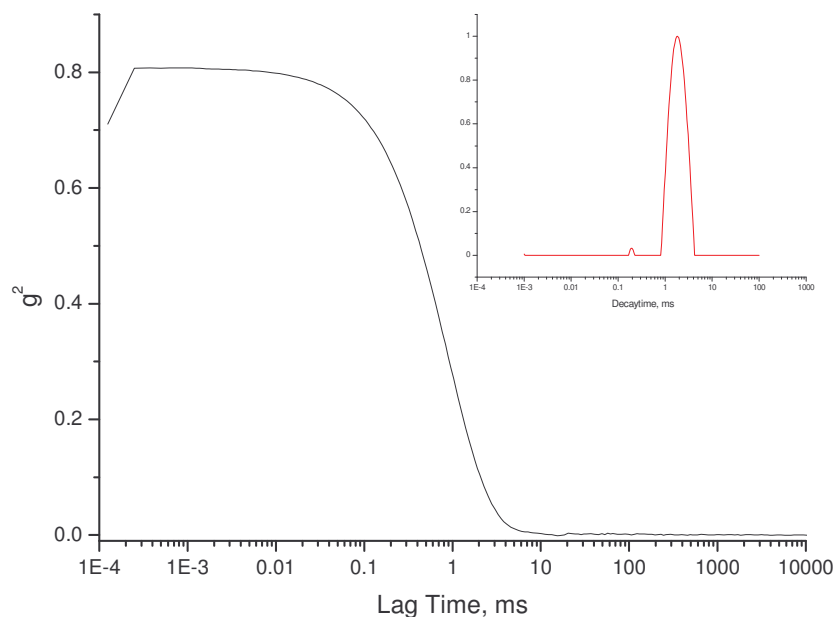
Figure 27 Correlation curve (90°, 5 minutes measurement time) at neutral pH before addition of NaOH. The small inset shows the contin fit of the correlation curve.

This phenomenon can partly be explained by recharging the lysine residues and their subsequent repulsive Coulomb interactions. On the other hand we have no reason to believe that the secondary structure of the β-helix is disturbed by changing pH conditions, and probably does not contribute to the change of supramolecular organization. Further evidence for the reversibility of the aggregation process is given by the fact that gramicidin does not bury its hydrophobic side chains in the interior of a tertiary structure. Thus, it does not aggregate because it unfolds, but due to a loss of charge.

We are aware that the secondary structure of poly-lysine changes from random coil to α-helical upon deprotonation. However, we do not believe this process contributes significantly to the observed phenomena because of the predominant influence of the lysine charges to the polarity of the peptides

Table 5: 2nd Order Cumulant Fit Data of gA-K$_6$ at 90°

|	Before basification	After basification
r$_H$	133.15	131.78
PdI	0.196	0.174
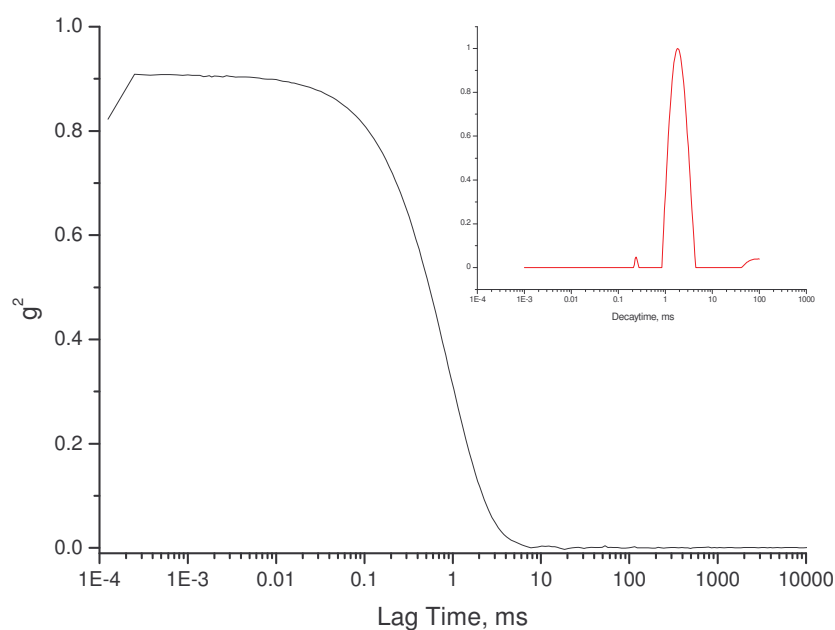
Figure 28 Correlation curve (90°, 5 minutes measurement time) at neutral pH after addition of NaOH. The small inset shows the lag time distribution calculated from the correlation function with the contin fit. Second order cumuland fit data is given in Table 5.

To approve the vesicular structure of the assemblies we encapsulated a fluorescent dye observed changes of the localized fluorescence upon pH dependent peptide aggregation.

Water soluble AlexaFluor 488 was encapsulated in gA-K$_6$ vesicles (Figure 29) as described in section 6.2.14 and exposed to pH 12. The dye was released upon sample aggregation since the localized fluorescence disappeared immediately after addition of NaOH. Therefore, we can exclude the aggregation of intact vesicles and conclude that precipitation occurs on the level of single molecules or dimers.

Figure 29 Base dependent release of an encapsulated fluorescent dye, observed by time dependent CLSM pictures. The pictures were taken in time intervals of 10 seconds.

4   Conclusion

We synthesized short amphiphilic peptides with 8 to 28 amino acids based on the hydrophobic sequence of gramicidin A. By reverse phase chromatography, we are able to obtain counter ion free samples with purity higher than 95 % and thus virtually without molecular polydispersity.
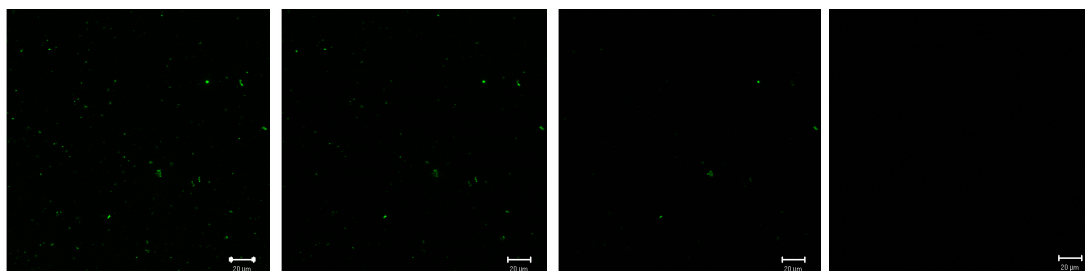
When the peptides are dissolved in ethanol and dialysed against water, they self-assemble partly to vesicular structures, partly to smaller objects. Their size and size distribution depends on manifold factors in sample preparation like exposure to higher temperature (annealing), choice of the organic solvent and addition of ions. Vesicles prepared by dialysis were lyophilized and analyzed by multiple microscopy techniques. The combined results indicate emerging evidence for the presence of membranes and hollow spherical structures. The rigidity of the vesicle membranes is unexpected and cannot be fully explained, yet there is support for the hypothesis that tryptophane residues aligned in a gramicidin typical helix secondary structure are able to interact and thus stabilize the membrane due to aromatic interactions[83] in addition to a hydrophobic effect. This hypothesis is further supported by the fact that the Trunk (Figure 30), consisting of the last seven amino acids of gramicidin in combination with at least one lysine residue is sufficient to form the same supramolecular features than gA.

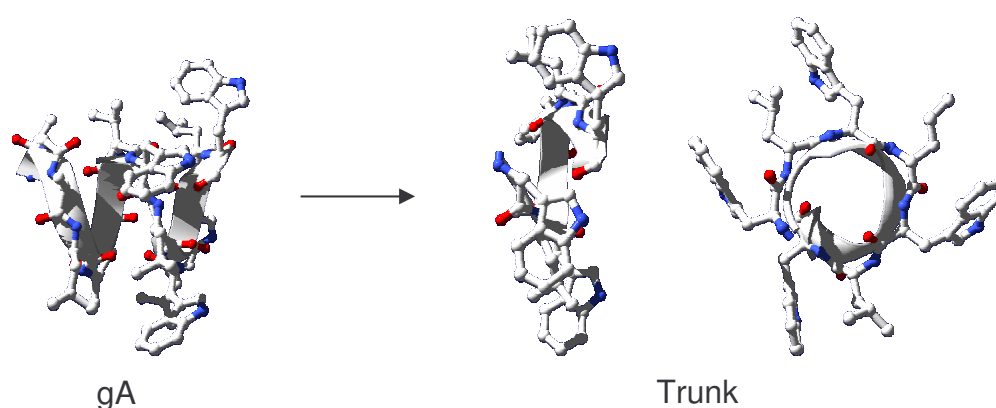gA   Trunk

Figure 30 Comparison of gA and Trunk structures, considering identical secondary structure (1GRM)

The ability to release the vesicle contents by destroying the membrane structure is unexpected because of the initially mentioned stability of the vesicles. However,

increasing the pH over the pK and thereby removing the positive charges of lysine greatly enhances the hydrophobicity of the peptides, leads to aggregation and thus release of the vesicle content. Neutralizing the pH leads to vesicle reassembly from the precipitated state and can be explained by the repulsive forces of charged lysine residues. Nevertheless, the monodisperse size distribution of the newly formed structures remains unambiguous.

Circular dichroism is a suitable method to study the correlation of sequence and structure of our molecules. As expected, the secondary structure of lysine corresponds to a random coil at neutral pH and shows systematic variation of ellipticity depending on the poly-lysine block length. Considering previous structural studies on wt-gramicidin we can conclude that our peptides do form dimers since gA and, even more the Trunk, are too short to exhibit distinct secondary structure without the ability to dimerize. Further, we know that the secondary structure (and therefore the dimerization pattern) of the Trunk derivatives is identical to the one from "full length" gA-molecules.

Due to the lack of reference data, CD delivers semi-quantitative information about the amount of secondary structure. The spectra we obtained reveal that helical structure is more pronounced in Trunk peptides than in gA, independently from the lysine chain length. By comparison of mean molar residue ellipticities between Trunk and gA we learn that the equilibrium constant of folding (K_f) of the Trunk is higher than K_f of gA, even though the latter has roughly double the mass. We can conclude that the first eight amino acids of gA do not promote but rather inhibit the formation of β-helical secondary structure.

Despite a great deal of CD studies already performed during the last decades it is not possible to assign a quaternary structure to our CD spectra, partly due to ambiguous resources, and probably also because of a slightly diverging secondary structure of our samples due to synthetic modifications as well as the self-assembled membrane state.

We can further conclude that there must be two hierarchies of quaternary structure; the first of which arising from the state of dimerization which, in case of our molecules, is responsible for the formation of "unimers" with amphiphilic ABA triblock character. The second hierarchy of quaternary structure is due to lateral unimer interactions and alignment of the ABA units. As mentioned earlier, the stability of those membranes can hardly be explained in terms of the hydrophobic effect, mainly

due to the limited size of the peptides and the absence of covalently crosslinked membrane constituents. Therefore, we propose aromatic interactions between tryptophane residues in addition to the amphiphilic sequence of our peptides as the key to the formation of the membrane super-structure
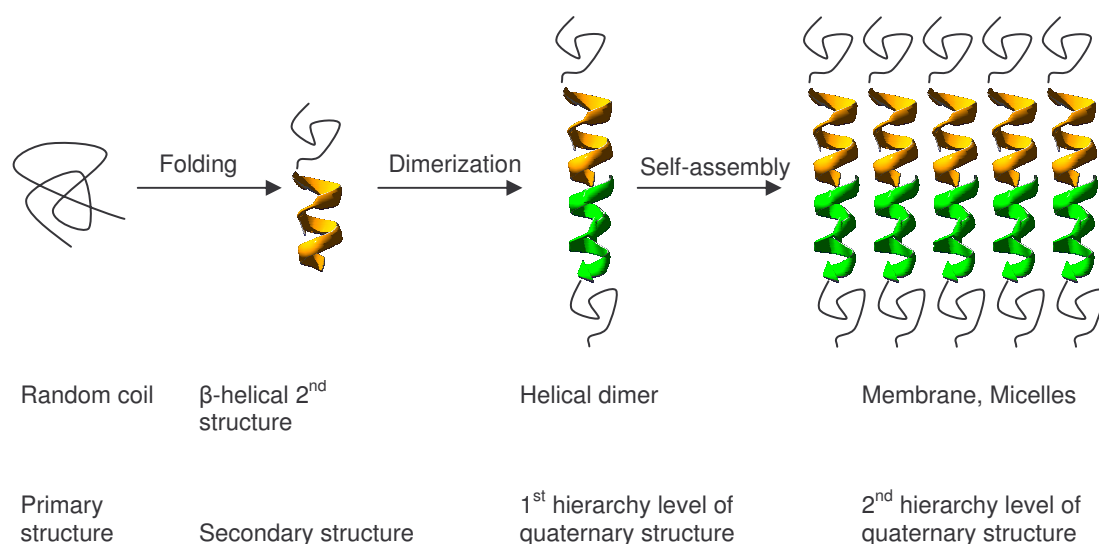

Random coil	β-helical 2nd structure	Helical dimer	Membrane, Micelles
Primary structure	Secondary structure	1st hierarchy level of quaternary structure	2nd hierarchy level of quaternary structure

Figure 31 Proposed steps from primary structure to membrane formation.

Gramicidin-helix based membranes are complex and versatile functional systems. To optimize the system for specific applications it will be necessary to understand the thermodynamic relations of structural and mechanical properties. The difficulty consists in the interdisciplinary character of the system: techniques from structural biology are difficult to apply due to the colloidal character of the samples and methods used in soft matter science can often not be applied because of the stability of the membranes. Main challenge of further peptide analytics will be to find proper methods.

CD spectroscopy by itself is not sufficient to elucidate the structural properties of the system. However, the addition of certain cations like Ca^{2+}[64] (promotion of double helical conformation) or Cs^+[84] which alters the secondary structure of double helices may give preliminary evidence of the precise dimerization state. Nevertheless, 2D-NMR needs to be applied to precisely resolve intramolecular interactions of functional groups.

To date, little is understood in our system about the the individual steps from peptide folding to the membrane self-assembly. The proposed structural features displayed in

Figure 31 needs to be confirmed by complementary structural resolution like 2D-NMR and X-ray crystallography. Furthermore, it will be important to obtain quantitative thermodynamic data about the intermediate steps of membrane formation; we need to obtain the equilibrium constants of folding, dimerization and the lateral dimer self-organization to membranes and micelles to study the response of the system to changing environmental parameters. Counter ions of charged lysine, monovalent cations in the gramicidin channel and divalent cations in between helical monomers need to be taken into account and might influence the equilibrium constants between different states of self-assembly. This will be necessary to obtain reaction enthalpies of intermediate steps, for example by isothermal titration calorimetry. Eventually, control about the thermodynamic properties of the system will allow us to relate the peptides' sequence to size and form factor of the assemblies by static light scattering measurements, further complemented by microscopy techniques.

5 Outlook

The properties of the peptides (and thus the structure of the membrane) can be changed at high resolution by the Insertion of amino acid point mutations in terms of stability and functionality. The compact symmetry of the Trunk-unit holds great promise to be up-scalable. Adding further pairs of D-leucine and L-tryptophane to the sequence of the Trunk might increase the stability of the membrane and allows attaching hydrophilic "loads" larger than 5 lysine residues.

In a preliminary experiment, monosaccharides were already coupled to the Trunk-sequence. Sugar coated vesicles might emerge to promising new vaccines. The key-lock-principle of the dimerization is a promising tool for surface experiments; cysteine-coupled gA or Trunk molecules can be attached to a gold surface and represent a regular pattern of specific binding sites for other gA or Trunk monomers. This way, an alternative to the docking mechanism of the biotin-streptavidin couple or DNA-hybridisation can be achieved, without the spatial constraints of streptavidin or the economical disadvantages of DNA. Moreover, specific lateral interactions of the tryptophane residues might enable us to design the surface pattern, for example by the choice of differing hydrophilic head groups or the insertion of point mutations in the helical part. This principle could be applied in an arbitrary alignment of RGD-sequences for specific cell-surface recognition.

Our peptide vesicles are also very promising containers for drug delivery since gramicidin is a membrane peptide and therefore soluble in lipid double layers. It is very likely that the interaction of gA-vesicles and cell membranes would induce a fusion process. Proper design of the peptides regarding biocompatibility and pH-sensitivity would allow a long circulation time in the blood stream and controlled release of the contents at the appropriate site, facilitated by the functionality of the peptide self-assemblies.

The material presented in this work demonstrates the progress made towards design of stable structures, which are biologically active and responsive to outside stimuli. Recently, the combination of experimental and theoretical methods has provided important insights into the physical behaviour of amphiphilic block-copolymer self-assembly. Due to this progress, the molecular toolbox has been augmented from purely lipidic systems to synthetic polymers, which outperform lipid membranes in terms of stability and load retention, eventually gaining functional diversity by the incorporation of peptidic components. Whereas pure lipid and synthetic membranes

can be mainly considered structural elements of transport vehicles, proteins and peptides introduce the potential to deploy biological function with the specificity needed to be applied in medicine.

6 Materials and Methods

6.1 Materials

For a detailed list of materials see Annex 7.1

6.2 Methods

6.2.1 Peptide Synthesis

All peptides were synthesized with a batch synthesizer on solid phase using Fmoc protection group chemistry. Rink Amide AM resin (loading: 0.4 – 0.8 mmole/g) was used as solid phase and all reactions were carried out in DMF as a reaction solvent (previously dried with Alox). Synthesis was performed with 200 mg of resin in a 10 mL syringe. The Fmoc protected amino acids were dissolved in DMF Alox (0.5 mol/L) prior to synthesis and the coupling reaction was carried out according to the protocol in Table 6.

The Fmoc protection group was cleft twice for each coupling step using 40% piperidin in DMF. HCTU was used as coupling agent and DIPEA dissolved in NMP as a base. All couplings were executed with 4 equivalents (eq) of amino acid, 4 eq of HCTU and 12 eq DIPEA relative to the resin loading. After each coupling step, the terminal amino group was capped by acetylation with a solution of 4 eq acetic anhydride and 5 eq of DIPEA in DMF alox.

The product was alternatingly washed three times with DMF respectively isopropanol and subsequently dried over night.

Table 6: Automated Steps of the Batch Fmoc Solid Phase Peptide Synthesis

Step	Reagent / Solvent	Repetitions	Time	Description
1	40% Piperidin/DMF	1	5 min	Fmoc deprotection
2	40% Piperidin/DMF	1	10 min	Fmoc deprotection
3	DMF	5	1 min	Wash
4	4 eq Fmoc protected AA 4 eq HCTU4 12 eq DIPEA 12 eq DIPEA	1	60 min	Coupling[*]
5	DMF	2	1 min	Wash
6	5 eq acetic anhydride 5 eq DIPEA	1	20 min	End capping[**]
7	DMF	3	1 min	Wash

[*] in DMF Alox / NMP
[**] in DMF Alox

6.2.2 *Cleavage From Resin*

Peptide cleavage from the resin and removal of protection groups was done with 95% TFA, 2.5 % Triethylsilane and 2.5 % H_2O. The ice cooled cleavage mixture was added to the resin and agitated during 120 min. Subsequently, the cleavage mixture was precipitated in 40 mL in ice cooled diisopropylether and centrifuged for 20 min at 9000 rpm. The supernatant was decanted, and the precipitated peptide redispersed in another 40 mL of diisopropylether. After another centrifugation (20 min, 9000 rpm) the residual crude product was dried over night in a desiccator.

6.2.3 *Preparative Purification (Reverse Phase HPLC)*

In the following, buffer A denotes 0.1 % TFA in bidistilled H_2O, buffer B stands for acetonitrile (ACN).

We purified all peptides on a Shimadzu Prominence HPLC. The peptide crude material was dissolved in 2 mL DMF, diluted with H_2O (0.1 % TFA) to a final volume of 20 mL and filtered through a 0.45 µm PTFE syringe filter. Peptides with shorter poly-lysine chains that are more hydrophobic in character were not always soluble in 10% DMF in water and needed addition of ACN to be kept in solution. Immediately after filtration the solution was pumped to a Merck LiChrospher 100, RP-18e (5 µm), 250-10 column at a flow rate of 4 mL/min by a sample pump (Shimadzu LC-20A). After 10 minutes of column equilibration time 5 mL/min on 5% buffer B the gradient was applied.

Table 7 shows the gradients from solvent A to solvent B applied for preparative and analytical HPLC runs.

Table 7: HPLC System Parameters

Step	Preparative	Analytical
System	Shimadzu Prominence	Shimadzu Prominence
Solvent A	H_2O bidist, 0.1% TFA or 2% AcOH	H_2O Bidist, 0.1% TFA
Solvent B	Acetonitrile	Acetonitrile
Column	LiChrospher 100, RP-18e(5µm), 250-10	LiChrospher 100, RP-18e(5µm), 250-4.6
Gradient	5% → 95 @ 120 min	5% → 95 @ 120 min
Injection	20[*] or 50[**] mL	25 µL
Flow	5 mL/min	1.5 mL/min
Detection	280 nm	280 nm
Fractionation	$\lambda > 500$ mAU	-
Fraction Size	5 mL	-

[*] TFA
[**] AcOH

The product was fractionated according to an absorption > 500 mAU at 280 nm and the collected fractions were analyzed qualitatively for mass by MALDI-TOF MS and quantitatively for purity by analytical HPLC. Fractions with more than 60 area % product peak were combined and diluted 1:1 with 2% acetic acid in H_2O and reapplied to the preparative RP-HPLC column (see Table 7), this time with 2% AcOH in the aqueous solvent A. The fractionation conditions in the second run and the analysis of the collected fractions were performed according to the first purification run; fractions with more than 95% product peak were combined.
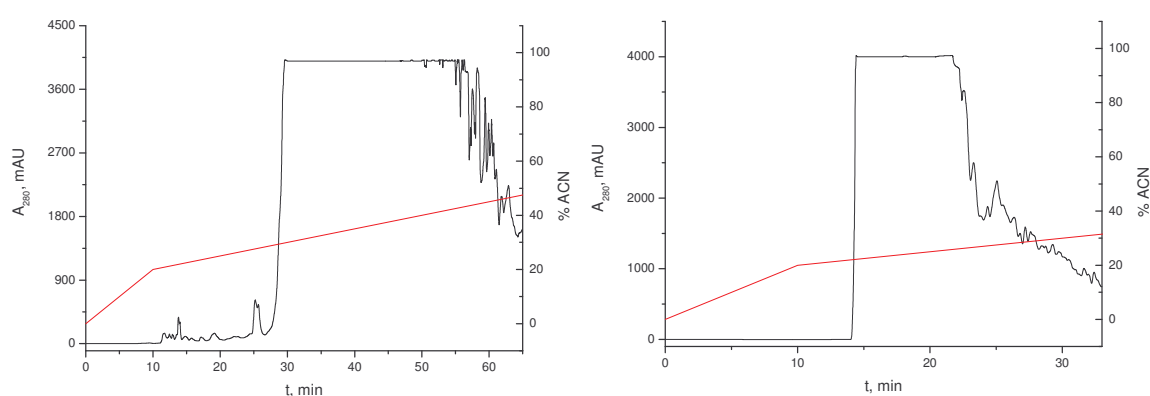

Figure 32 Left: Elution diagram of the first pereparative RP-HPLC run (TFA). Right: Second preparative RP-HPLC run (AcOH) after collection of fractions with > 70 area percent.

6.2.4 *Product Characterization and Determination of the Sample Concentration*

Purity analysis and quantification of the sample concentration was determined by analytical HPLC (RP-18e (5µm), 250-4.6) and calculated by the ratio of product peak integral to the overall integral of the elution diagram (Figure 33). The system parameters of the analytical HPLC is given in Table 7.

Sample concentrations were determined by analytical HPLC (RP-18e (5µm), 250-4.6). 25 µL of sample solution were diluted 1:1 with ACN and passed through a 0.45µm PTFE syringe filter. We used an external standard, calibrated on the molar concentration of gA- and Trunk-derivatives at five concentrations.

The peak integral values are fitted linearly by following equations:

Trunk: $\qquad y = 5.88786 \cdot 10^{-8} x + 0.0021 \qquad\qquad R^2 = 0.99987$

gA: $\qquad\quad y = 5.56154 \cdot 10^{-8} x + 0.0051 \qquad\qquad R^2 = 0.99955$
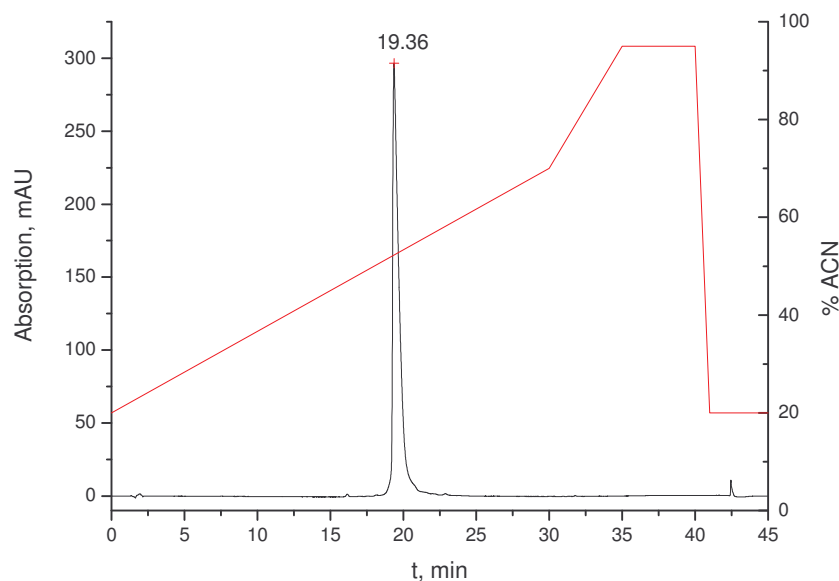
Figure 33 Analytical HPLC elution diagram of gA-K$_6$. For detailed system parameters see Table 7.

6.2.5 *Elimination of Counter Ions*

TFA$^-$-counterions were eliminated by the second preparative RP-HPLC step carried out with 2% acetic acid in the aqeous phase. AcO$^-$ in turn, as a counterion of the cationic peptides, was eliminated by repeated addition of ammonia prior to lyophilisation according to this protocol:

1. Addition of ammonia to pH 11 and lyophilization
2. Dissolution in 40 mL 30% ACN in bidistilled H$_2$O, addition of ammonia to pH 11 and lyophilization.
3. Repetition of step 2.
4. Dissolution in 40 mL 30% ACN in bidistilled H$_2$O and lyophilization.
5. 2 repetitions of step 4

6.2.6 *MALDI-TOF-MS*

Determination of the product mass and a first estimate of the sample purity was performed by mass spectroscopy; 0.8 µL of sample solution (c ~ 1mg/mL) was applied to a gold sample plate and mixed with 0.8 µL of matrix solution (1 mg/mL *α*-cyano-4-hydroxycinnamic acid (dissolved in a 1:1 mixture of ACN to H$_2$O (0.1% TFA)). The spectra were taken in reflector mode with positive polarity and manual

acquisition control. The grid voltage was set to 75%. 400 to 600 laser shots were averaged (Figure 34). Additional settings are given in Table 8.
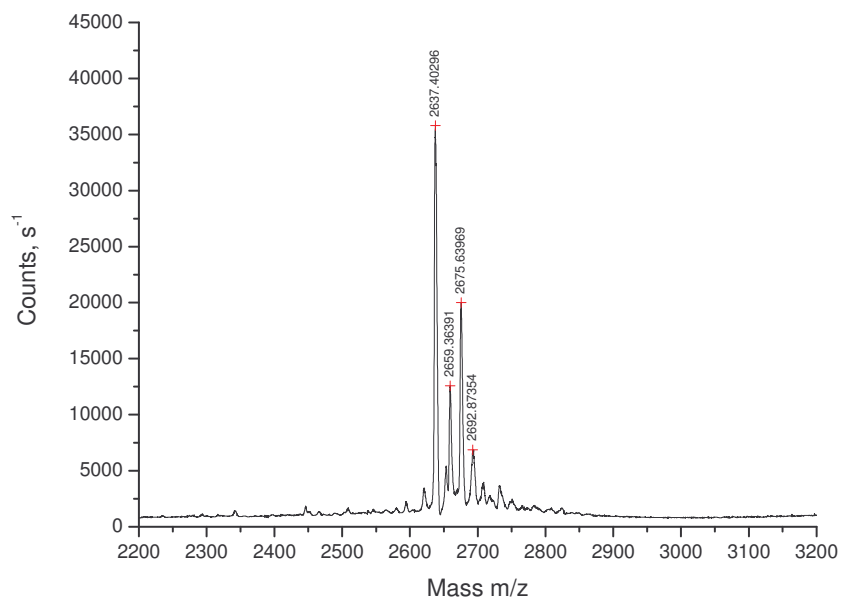

Figure 34 MALDI-TOF-MS of gA-K$_6$

Table 8: MALDI-TOF System Parameters

Parameter	Value
Accelerating voltage:	24000 V
Grid voltage:	75%
Mirror voltage ratio:	1.12
Guide wire 0:	0.1%
Extraction delay time:	50 nsec
Acquisition mass range:	500 - 3000 Da
Number of laser shots:	100/spectrum
Laser intensity:	usually around 2000 +/- 100
Laser Rep Rate:	20.0 Hz
Calibration type:	Default
Calibration matrix:	α-Cyano-4-hydroxycinnamic acid
Low mass gate:	Off
Timed ion selector:	Off
Digitizer start time:	20.5435
Bin size:	0.5 nsec
Vertical scale 0:	500 mV
Vertical offset:	0.5%
Input bandwidth 0:	500 MHz

6.2.7 *Membrane Self-Assembly*

Peptides were dissolved in a solution of 1.9 mL EtOH and 0.1 mL 2M HCl at a concentration of 0.5 to 2 mg/mL. Subsequently, the mixture was dialyzed (CE, 1000 Da cutoff) three times against 1 L of H_2O bidist.

6.2.8 *Circular Dichroism*

We used 1 mm path length QS cuvettes to minimize solvent absorption effects. Blank measurements were carried out in the appropriate solvents immediately prior to the sample measurements. The sample concentrations were adjusted according to a HT voltage in between 300 and 460 V in the far-UV range. Each spectrum was averaged from three scans with 1 nm-intervals, for each the signal was averaged for 3 seconds. Unfolding studies on CD were performed with a heating rate of 1 K/min from 20 to 80 °C and back again to 20 °C. The ellipticity was determined at 223 nm and recorded in intervals of 1 K.

6.2.9 *Dynamic Light Scattering*

We used an ALV/CGS-8F platform based goniometer system equipped with an ALV/-5000/E correlator and an Argon-Ion laser with a wavelength of 633 nm (35mW). Correlation functions were fitted with the ALV-correlator software by the cumulant function and the contin algorithm. Concentration dependencies and multiple scattering effects were minimized by extrapolation to 0°.

6.2.10 *Atomic Force Microscopy*

Peptide samples were prepared according to section 6.2.7 and applied to a mica support. Measurements were carried the solid-air interface in tapping mode, and a cantilever spring constant of 42 N/m.

6.2.11 *Transition Electron Microscopy*

We used 400 mesh Cu-grids coated with 8 nm carbon film. The grids were cleaned in O2 plasma before the application of the samples.

20 µL of peptide sample (ca. 1 mg/mL) was applied on the grids for 1 minute and washed 2 times with MilliQ water and subsequently stained with 1% uranyl acetate. We applied a voltage in between 80 and 100 kV for the measurements.

6.2.12 *Scanning Force Microscopy*

gA-K$_8$ and Trunk-K$_3$ samples were prepared according to section 6.2.7. Dialysed samples were lyophilized in 1 mL Eppendorf tubes and vaporized with a gold or platimium layer.

6.2.13 *pH Dependent Aggregation*

Peptide samples were prepared as described in section 6.2.7. DLS was performed in between 30° to 150° with 10° steps with 5 minutes measurement time each. The samples were then dialyzed against 800 mL of H$_2$O bidist with pH 12. After that we dialyzed the samples against 800 mL H$_2$O bidist at pH 3 and 2 times against H$_2$O bidist at pH 7 with a subsequent DLS measurement according to the protocol in section 6.2.9.

6.2.14 *Encapsulation of a Fluorescent Dye*

gA-K$_6$ was dissolved in 950 µL EtOH and 100 µL 2M HCl passed through a 0.45 µm CE filter. The sample was in two parts; 50 µL AlexaFluor 488 (140 µM in H$_2$O) was added to the first half, the second half was mixed with 100 µl Rhodamin 6G (2.06 µM in EtOH). 1.5 mL H$_2$O bidist was added to both samples and subsequently dialyzed 3 times against 800 mL H$_2$O bidist (Spectra/Por® Biotech CE, MWCO: 1000 Da). The resulting solutions were analyzed by CLSM. During the experiment we added 10 µL of 1M NaOH to 100 µL sample solution. After 15 min 11 µl 1M HCl was added and a DLS measurement at 90° was performed for 5 minutes.

6.2.15 *Antibacterial Effect*

The antibacterial effect of our samples was tested on wild type of gram-positive Staphylococcus aureus (SA113 wt) and the mutant SA113 ΔdltA which is very sensitive to cationic antimicrobial peptides. 1 mg of gA-K$_6$ and Graamicidin D were prepared each according to the prorocol in section 6.2.14. Sterile 96-well microtiter

plates were doped with SA113 wt respectively SA113 ΔdltA on 1000 CFU/ml in 100µl Müller-Hinton-Broth (MHB). The alleged antibacterial test substances were applied according to a dilution series: gramicidin D (0 to 50 µg/mL) and gA-K$_6$ (0 to 50 µg/mL). The sample plates were incubated for 24 h at 37 ℃. The minimal inhibition concentration (MIC) is defined as the lowest concentration of the antibiotic where no bacterial growth can be detected anymore. Bacterial growth was observed by determination of the optical density at 590 nm. The minimal bactericidal concentration (MBC) is the lowest concentration of the antibiotic where no bacteria do survive and was detected by plating the samples on a Müller-Hilton culture medium. The results can be found in Annex 7.2.3.

7 Annex

7.1 Materials

7.1.1 Chemicals

Rink Amide AM resin (200-400 mesh), Novabiochem 01-64-0038

N,N-Dimethylformamide (DMF), purum, ≥ 99.9% (GC), JT.Baker 7032

Aluminium Oxide, Merck 1078

Dichloromethan, rein, Schweizerhall 81830-156

Piperidine, purum, ≥ 96.0% (GC), Fluka 80642

N,N-Diisopropylethylamine, 99%, Aldrich D12,580-6

HCTU: (O-(6-Chlorobenzotriazol-1-yl)-N,N,N′,N′-tetramethyluronium hexafluorophosphateuka), 99.7%, Iris Biotech GmbH 330645879

Fmoc-Ala-OH, ≥ 98.00% (HPLC), Novabiochem 04-12-1006

Fmoc-Glu(OtBu)-OH, ≥ 98.00% (HPLC), Novabiochem 04-12-1020

Fmoc-Gly-OH, ≥ 98.00% (HPLC), Novabiochem 04-12-1001

Fmoc-Lys(Boc)-OH, ≥ 98.00% (HPLC), Novabiochem 04-12-1026

Fmoc-Leu-OH, ≥ 98.00% (HPLC), Novabiochem 04-12-1025

Fmoc-D-Leu-OH, ≥ 98.00% (HPLC), Novabiochem 04-13-1025

Fmoc-Val-OH, ≥ 98.00% (HPLC), Novabiochem 04-12-1039

Fmoc-D-Val-OH, ≥ 98.00% (HPLC), Novabiochem 04-13-1039

Fmoc-Trp(Boc)-OH, ≥ 98.00% (HPLC), Novabiochem 04-12-1103

Acetic anhydride, purum, Synopharm 0107700

Trifluoroacetic acid (TFA), ≥ 98.0%(T), Fluka 91700

Triethylsilane (TES), 97%, Fluka 90550

Diisopropyl ether, purris. p.a. ≥ 98.0%, Fluka 38279

Acetonitrile, HPLC Grade ≥ 99.9%, Fisher Chemicals A/0626/17

Acetic acid, glacial, 100%, VWR ProLabo 84 528.290

α-Cyano-4-Hydroxycinnamic Acid (CCA), 97%, Aldrich 14,550-5

Ethanol, 96% EP, Schweizerhall 82352-102

gramicidin A, BioChemika, ≥ 90.0% (HPLC), Fluka 50845

Pyridin, ReagentPlus, ≥ 99.0%, Fluka 320498

2,2,2-Trifluoroethanol, puriss., ≥99.0% (GC), Fluka 91690

1-Methyl-2-pyrrolidinone (NMP), for peptide synthesis, ≥ 99.5% (GC), Fluka 69116

1,4-Dioxan, puriss., absolute, over molecular sieve, ≥ 99.5% (GC), Fluka 42510

Chloroform, anhydrous, amylenes as stabilizer, ≥ 99%, Aldrich 372978

Alexa Fluor® 488 C_5 maleimide, Invitrogen A10254

Rhodamine 6G chloride, Invitrogen R634

7.1.2 *Machines*

Peptide synthesizer Syro 1 MultiSynTech

Centrifuge, U_{max}=4500U/min, r=10cm, V_{max}=300ml

HPLC: Shimadzu Prominence 20A HPLC-System

MALDI-TOF-MS: PerSeptive Biosystems Voyager-DE Pro, Biospectrometry Workstation

Lyophilizer: Heto Maxi Dry Lyo

Langmuir Blodgett: KSV Instruments Ltd., 432 cm^2 PTFE trough

Brewster Angle Microscopy: BAM2plus, Nanofilm Technologie GmbH, Nd:YAG Laser (532nm)

Light Scattering: ALV/CGS-8F Platform based Goniometer System, ALV/-5000/E Correlator with a Argon-Ion Laser (633nm 35mw)

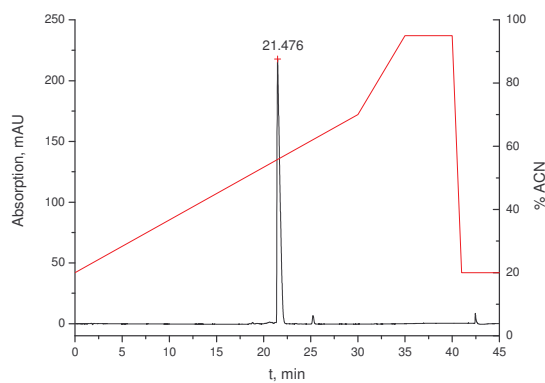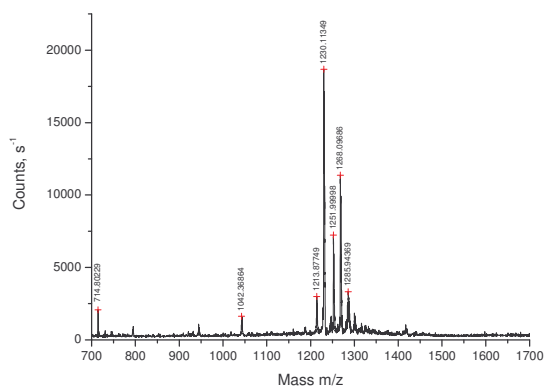Confocal Microscope: ZEISS LSM 510 META with FCS Confocor 2

REM: High Resolution field emission scanning electron microscope, Hitachi S-4800

TEM:
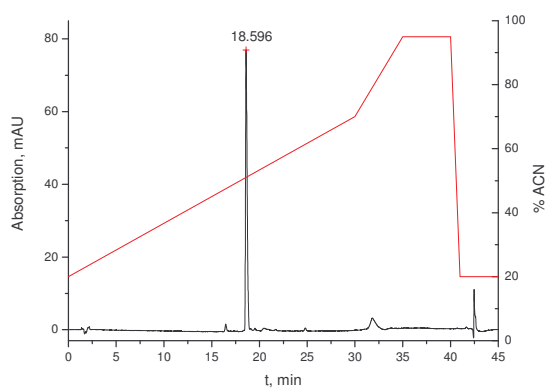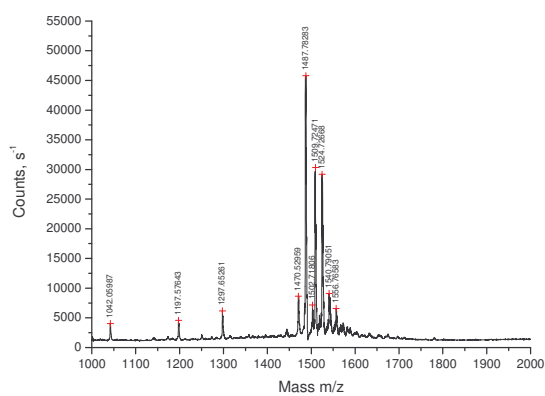
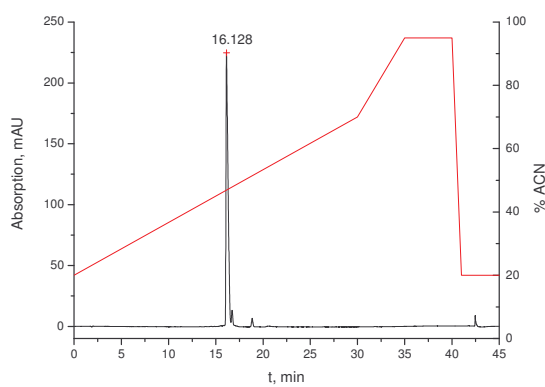CD: Applied Photophysics Chirascan CD-Spectrometer

7.2 Additional Results

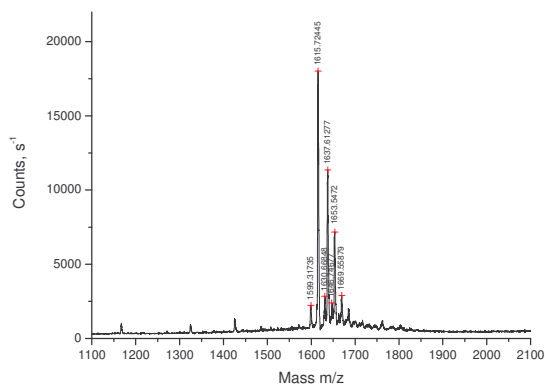## 7.2.1 Product Characterization (MS / HPLC)

Trunk-K$_1$

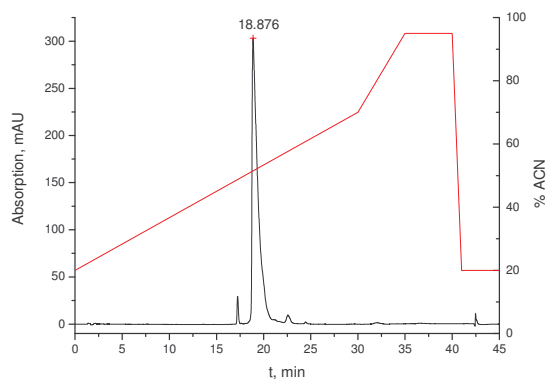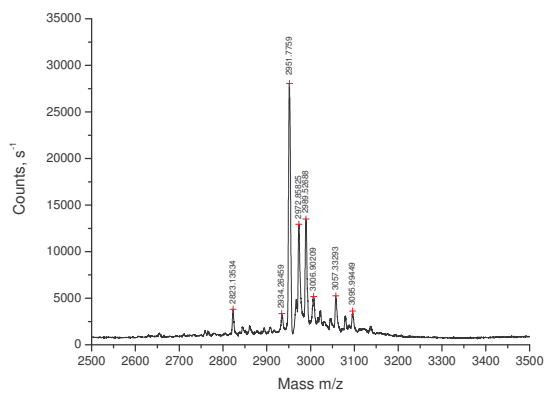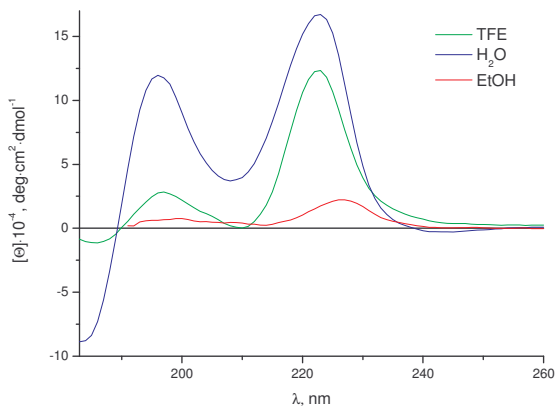Trunk-K$_2$

Trunk-K$_4$
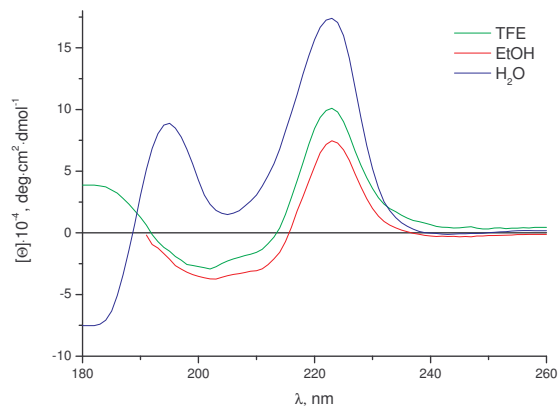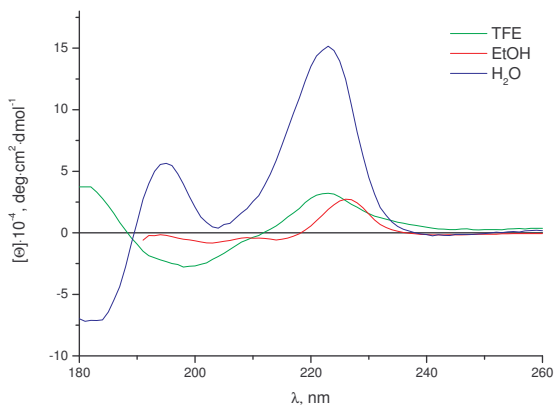
gA-K$_2$

gA-K$_4$

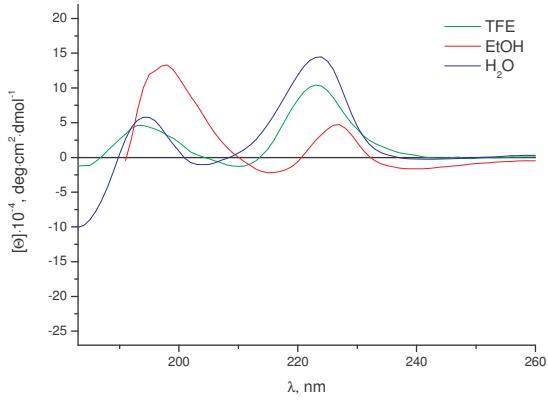gA-K$_6$

gA-K$_8$

7.2.2 *Solvent Dependent Circular Dichroism*

Trunk-K$_1$

Trunk-K$_2$

Trunk-K$_3$
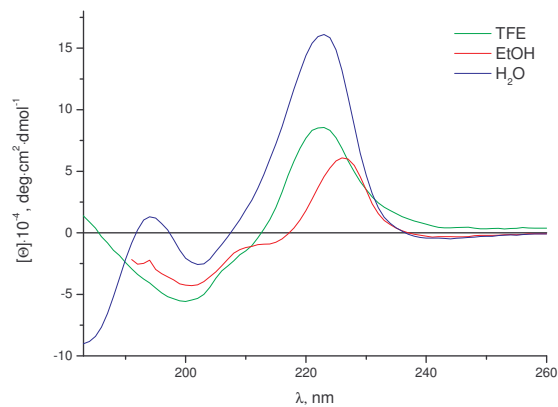
Trunk-K$_4$

gA-K$_2$
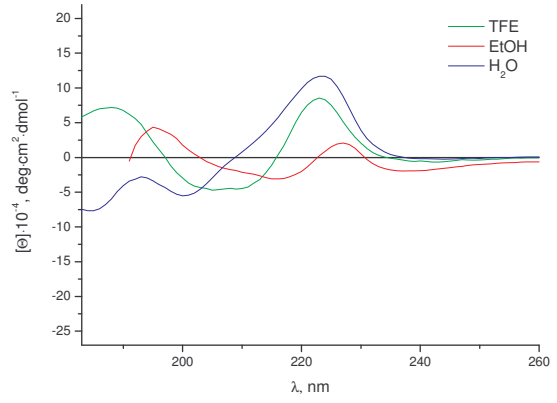
gA-K$_4$

gA-K$_6$

gA-K$_8$

gA-K$_{10}$

66
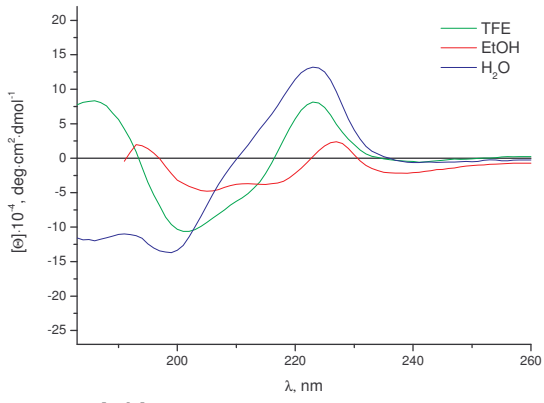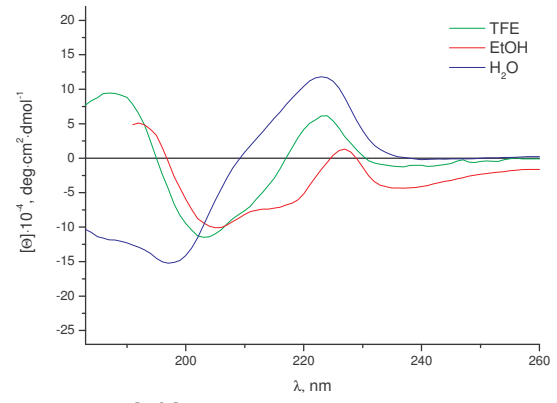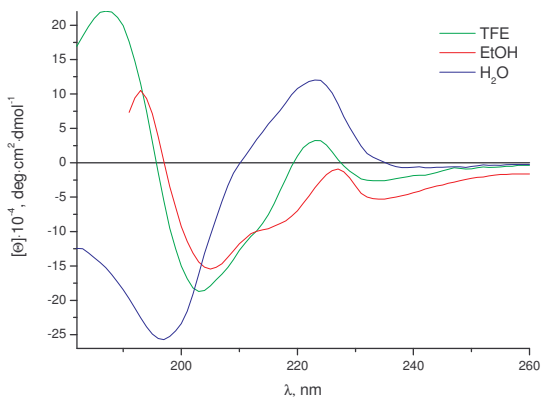
7.2.3 *Antibacterial Activity*

	OD(590)	
Gramicidin D	SA113 wt	SA113 ΔdltA
50.00	0.044	0.048
25.00	0.043	0.039
12.50	0.052	0.041
6.25	0.407	0.060
3.13	0.259	0.179
1.56	0.243	0.172
0.78	0.260	0.164
0.39	0.265	0.161
0.20	0.261	0.166
0.10	0.282	0.145
bacteria in me	0.317	0.231
medium	0.043	0.048

	OD(590)	
DdB-4/1d (µg	SA113 wt	SA113 ΔdltA
50.00	0.052	0.052
25.00	0.045	0.043
12.50	0.042	0.042
6.25	0.399	0.096
3.13	0.300	0.194
1.56	0.267	0.157
0.78	0.257	0.176
0.39	0.257	0.170
0.20	0.242	0.169
0.10	0.241	0.183
bacteria in me	0.307	0.221
medium	0.038	0.039

	OD(590)	
DdB-6/1d (µg	SA113 wt	SA113 ΔdltA
50.00	0.660	0.059
25.00	0.156	306.000
12.50	0.235	0.045
6.25	0.280	0.218
3.13	0.253	0.176
1.56	0.254	0.208
0.78	0.233	0.184
0.39	0.261	0.189
0.20	0.219	0.158
0.10	0.220	0.157
bacteria in me	0.320	0.171
medium	0.044	0.048

	OD(590)	
EtOH/HCl (bla	SA113 wt	SA113 ΔdltA
1:10 (in MHB)	0.255	0.040
1:20	0.321	0.244
1:40	0.322	0.247
1:80	0.306	0.241
1:160	0.308	0.247
1:320	0.281	0.251
1:640	0.271	0.234
1:1280	0.229	0.236
1:2540	0.214	0.231
1:6080	0.253	0.222
medium	0.039	0.038

S. aureus wt and ΔdltA are not inhibited in growth in EtOH/HCl at used concentrations

Results

Gramicidin D	MIC (µg/mL)	MBC (µg/mL)
SA113 wt	12.50	> 50.00
SA113 ΔdltA	6.25	50.00

DdB-4/1d	MIC (µg/mL)	MBC (µg/mL)
SA113 wt	12.50	> 50.00
SA113 ΔdltA	12.50	50.00

DdB-6/1d	MIC (µg/mL)	MBC (µg/mL)
SA113 wt	>50.00	>50.00
SA113 ΔdltA	12.50	50.00

Vesicle-Monolayer Interaction of POPS/POPC Mixtures: A Model for Biological Fusion Processes

Christian Dittrich, Katarzyna Kita-Tokarczyk, Wolfgang P. Meier*

 University of Basel, Departement of Chemistry, Klingelbergstr. 80, 4056 Basel, Switzerland

wolfgang.meier@unibas.ch

Vesicle-Monolayer Interaction

Phone: +41612673802. Fax: +41612673855

The fusion behavior of unilamellar liposomes with a planar lipid Langmuir film was investigated by surface pressure measurements. Complemented by Brewster angle imaging and UV-Vis spectroscopy the method provides a straightforward and aggregation-insensitive approach to quantitate membrane fusions. Additionally, it does not require incorporation of other species such as fluorescent probes. The present work concentrates on the POPS-POPC system triggered for fusions by calcium ions, however, the experimental concept could be applied to any amphiphiles. Surface pressure changes of a lipid Langmuir monolayer during the aggregation and subsequent fusion with vesicles in the subphase are described. We discuss the observed phenomena in terms of varying vesicle concentration and lipid composition.
POPS, POPC, Fusion, Langmuir Monolayer, Calcium, Vesicle, Liposome

Introduction

Membranes in biological systems have the ability to separate and merge in order to take up, transport and release molecules. The exchange of distinct compartments along the endocytic and/or secretory pathway or over the synaptic cleft depends on a stunningly concise and reliable transport system.

The concept of such a discrete transport and delivery compartment is of great interest for medical applications. Hence, during the last decades, much attention has been paid to artificial vesicle systems to mimic Nature's vesicle fusions, but the necessary combination of stability and functional versatility emerged notably difficult to achieve. Even though the cellular processes of budding and fusion seem to collude in an intriguingly simple manner, the detailed molecular mechanisms are still subject of current investigations. Many factors like membrane composition, curvature, phase separation behavior and lipid-protein interaction influence the vesicular transport processes in cells.

It is essential to refer to concise observations of fusion events to understand them. Even though experimental models were reduced in complexity to vesicle-vesicle fusions, reliable and quantitative observations of fusion processes still remain an experimental challenge.

Fluorescent molecules and resonance energy transfer emerged as feasible probes and a measure for lateral distances within membranes[85-87] or vesicles' aqueous content.[88-90] Proper application of such probes can provide an insight into the dynamics of membrane mixing, content mixing as well as the efficiency of the fusion process (leakage).[88, 89, 91] However, resonance energy transfer measurements of fusions are demanding to evaluate quantitatively because the change of emitted light intensity is not linearly related to the extent of membrane or content mixing;[92] the detectable degree of fusion is limited by the Förster radius of the fluorophores.[92, 93] Moreover, fluorescent probes might interact with their surroundings and as a result bias membrane stability and fusion kinetics.[94-96]

Thus, it is desirable to supplement the existing fusion assays with a quantitative approach that does not depend on molecular probes. The objective of this work was to study the interaction of liposomes in solution with a lipid Langmuir film regarding fusions. The curvature asymmetry of this experimental setup gives an insight into the behavior of large unilamellar vesicles facing a much larger membrane-bounded object like a cell or even the negative membrane curvature of an endocytic vesicle's interior. Moreover, changes in surface pressure of a Langmuir film are a physical property that allows for kinetic mass transport studies.

Several studies about the interaction of vesicles with the air-water interface were carried out using the surface pressure measurements; Schindler[97] was the first who theoretically described the measurements of a monolayer formation from vesicles in solution. Mitev et

69

al.[98] introduced a theoretical steady-state approach with aggregated vesicles as intermediate species. Gugliotti et al.[99] studied the fusion and consequent monolayer formation from mixed PC and DODA(X) (dioctadecylamine) vesicles as a function of temperature and vesicle size. Fenzl et al.[100] investigated the surface of sonicated DMPC (1,2-dimyristoyl-sn-glycero-3-phosphocholine) suspensions in water by means of X-ray-reflectivity as a function of temperature and time. However, to our knowledge no publication so far focused on Langmuir films as a precondition for liposome-interface interactions to imitate cellular fusion processes.

In this work, the monolayers and vesicles consisted of POPS and POPC lipids since the negatively charged POPS can be triggered for fusion by an appropriate concentration of divalent cations. Calcium has a high efficiency to induce fusions of PS-containing membranes,[101] and the calcium concentration used in this work (5 mM) was found to be sufficient to induce fusions of PS-PC membranes.[102] The fusion efficiency of this system is independent of the membrane curvature[101] which is a prerequisite when interactions between planar and curved membranes are studied.

The system allows a change of the membrane net charge by variation of the POPS to POPC ratio in order to alter the fusion properties. We are aware of the fact that, due to strong asymmetry of the dielectric constants of air and water, a Langmuir monolayer is just a model of a biological lipid bilayer. However, considering similar lateral densities of lipid molecules in both systems,[103] the initial steps of a fusion process are assumed comparable.

Abundant documentation about the fusion behavior of POPS as well as POPS/POPC vesicles studied by resonance energy transfer serves as reference for this work.[104-107]

1. Materials and Methods

2.1 Materials

1-palmitoyl-2-oleoyl-sn-glycero-3-[phospho-L-serine] (sodium salt) (POPS) and 1-palmitoyl-2-oleoyl-sn-glycero-3-phosphocholine (POPC) were purchased from Avanti Polar Lipids (Alabama, USA). L-histidine (L-Hist, ultra, $\geq$ 99.5%), n-[tris(hydroxymethyl)methyl]-2-aminoethanesulfonic acid 2-[(2-hydroxy-1,1-bis(hydroxymethyl)ethyl)amino]ethanesulfonic acid (TES, ultra, $\geq$ 99.5 %), ethylenediaminetetraacetic acid (EDTA, ultra, $\geq$ 99.5 %), chloroform (puriss., $\geq$ 99.8 %) and ethanol (purum, $\geq$ 99.8 %) were obtained from Sigma (St. Louis, MO) and CaCl2 (ultra, $\geq$ 99.5) as well as NaCl (purum, $\geq$ 99.5) were bought from Fluka. Milli-Q water was used for buffer preparation and cleaning the Langmuir troughs.

2.2 Preparation of Unilamellar Vesicles

Large unilamellar vesicles (LUV) were obtained by the film hydration method; lipids dissolved in chloroform were dried on a rotary evaporator and applied to a vacuum line overnight. The resulting lipid film was hydrated in a calcium free buffer (further denoted as "standard buffer"[88]) consisting of 2 mM L-Hist, 2 mM TES, 0.1 mM EDTA and 54 mM NaCl, pH 7.4 to a final lipid concentration of 2.64 mM or ca. 2 mg·mL^{-1}. The mixture was vortexed for ca. 15 minutes and freeze-thawed 5 times from -190 to 40 °C. Subsequently, the suspension was extruded 12 times (Lipex^{TM} Basic Barrel Extruder, Northern Lipids, Canada) at 17 bars (N$_2$) and at room temperature through a 0.1 μm polycarbonate membrane (Whatman Nucleopore, England). The size and polydispersity of the resulting vesicles was determined by dynamic light scattering with an ALV (Germany)-500 Multiple Tau Correlator equipped with a 632 nm laser. The vesicles were protected from light, stored under argon and used within one working day.

2.3 UV-Vis Measurements

Turbidity measurements were carried out on a UV-Vis spectrophotometer (Safas mc^2, Monaco) at 600 nm and 20 °C. 33 μL of 305 mM CaCl$_2$ in standard buffer (adjusted to pH 7.4) were added to 2 mL vesicle solution and thoroughly mixed with a pipette. All time dependent measurements were started 20 seconds after the calcium addition, with the first measured value being a reference value. No stirring was applied during the experiments.

The fusion process was stopped and aggregation was reversed by addition of 33 μL 610 mM EDTA (adjusted to pH 7.4 in standard buffer).[89, 108] The solution was vigorously pipetted during one minute to disrupt residual aggregates.

2.4 Surface Pressure Measurements

2.4.1 Surface Pressure-Area Isotherms

Surface pressure-area isotherms of a POPC/POPS film in a ratio of 4:1 were measured on a Teflon^{TM} Langmuir trough (KSV Mini LB, Finland), total area 274 cm^2, equipped with two moving barriers and a clean piece of chromatography paper (ashless Whatman Chr 1) as a Wilhelmy plate. The trough was cleaned by successive wiping with chloroform and ethanol, and thoroughly rinsed with Milli-Q water. 15 μL of a 1.5664 mM lipid solution were spread on the buffer surface. 15 minutes after spreading, the isotherms were recorded at the compression rate of 5 mm/min. Measurements were carried out at 20 °C with standard and

calcium containing buffers (2 mM L-Hist, 2 mM Tes, 0.1 mM EDTA, 54 mM NaCl and 5 mM CaCl$_2$) as subphases.

2.4.2   Kinetics

The kinetic measurements were performed at 20 °C in a round Teflon^{TM} trough with an inner diameter of 6 cm and a height of 3.5 cm, cleaned in the same way as described above. The trough was filled with 60 mL standard buffer, constantly stirred by a small magnetic stirrer at 120 rpm. The lipid monolayer was spread from a chloroform solution to the initial surface pressure of 20 mN/m. After chloroform evaporated (15 min), 2 mL of vesicle solution were injected into the subphase through a channel, which connects the upper rim with bulk liquid to bypass the Langmuir monolayer, and stirred for 5 minutes. The fusion process was then induced by injection of 1 mL 315 mM CaCl$_2$ in standard buffer. In a control measurement, the influence of subphase level changes on the surface pressure readings was found negligible.

2.5   Brewster Angle Microscopy

A BAM2plus Brewster angle microscope (Nanofilm Technologie GmbH, Göttingen, Germany) with Nd-YAG laser at 532 nm, Nikon 10x Plan Epi SLWD objective (N.A. 0.30) and monochrome CCD camera attached to real-time frame grabber) was used to visualize the monolayers. The images were captured in line scan mode and corrected for geometry and contrast.

2.   Results and Discussion

3.1 Preliminary Experiments

3.1.1   Size and Dispersity of the Liposomes

The size distribution of vesicles was measured by dynamic light scattering at 90°. The mean vesicle hydrodynamic radius was 67 nm and the polydispersity amounted for 0.05. The correlation function was fitted by a second order cumulant. By virtue of this narrow vesicular size distribution the starting conditions of the fusion experiments were considered reproducible.

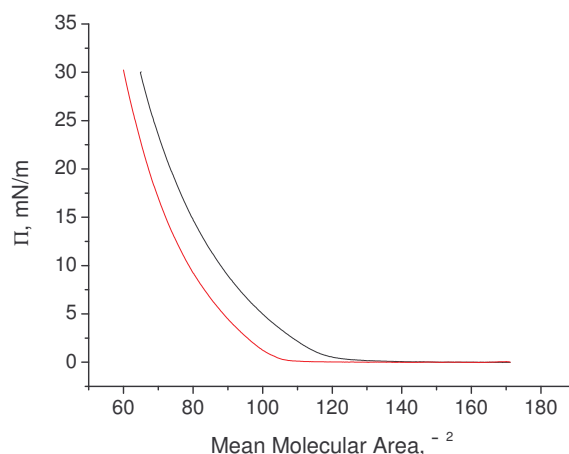### 3.1.2   Surface Pressure – Area (Π-A) Isotherms

Figure 1. Π-A-Isotherms of POPS/POPC monolayers in a molar ratio of 4:1. The subphase was standard buffer (black line) and standard buffer containing 5 mM $CaCl_2$ (red line).

Compression isotherms of Langmuir films were recorded to estimate the influence of calcium ions on the surface pressure of membranes consisting of POPS and POPC. Figure 1 shows two isotherms of POPS and POPC in the ratio of 4:1. The lipid film is stable over the time of the experiments and there are no visible phase transitions in the experimentally relevant surface pressure range between 10 and 30 mN/m (see 3.2.1), independently of the presence of Ca^{2+} ions. Calcium decreases the lipid molecular area and causes the monolayer to condensate. This phenomenon was discussed earlier[107] and is in agreement with our results.

3.2 Fusion Experiments

The conditions of the kinetic experiments were designed in order to verify the basic assumptions about calcium-induced phosphatidylserine dependent vesicle-vesicle fusions: the aggregation rate of POPS-containing vesicles is supposed to be faster than the fusion rate[101] and the lipid membrane material from the bulk should not significantly interact with the monolayer as long as no Ca^{2+} is added. The surface pressure measurement should remain insensitive to any processes in the bulk and to monolayer-vesicle aggregation when no material transfer takes place. Furthermore, variation of the initial vesicle concentration in solution should influence the fusion rate and as the last assumption, altering the molar ratio of POPS/POPC should change the overall surface charge and therefore the fusion kinetics.

Stirring was applied to avoid diffusion controlled fusion kinetics.[109] The stirring rate was determined slow enough not to influence the integrity of the Langmuir film (stable surface pressure conditions without the addition of vesicles during one hour).

3.2.1 Variation of the Vesicle Concentration

To validate the assumptions about our experimental setup the concentration of vesicles was linearly varied whereas membrane composition and all the other experimental conditions were kept constant. Figure 2 shows the change of surface pressure over time. Π sharply decreases by 6 mN/m shortly after the addition of 5 mM $CaCl_2$. This observation mirrors the condensation effect resulting from the interaction between Ca^{2+} ions and the negatively charged phosphatidylserine head groups.[110, 111] It is remarkable that calcium-caused decreases in surface pressure during kinetic experiments and compression isotherms are nearly identical (Figure 3).
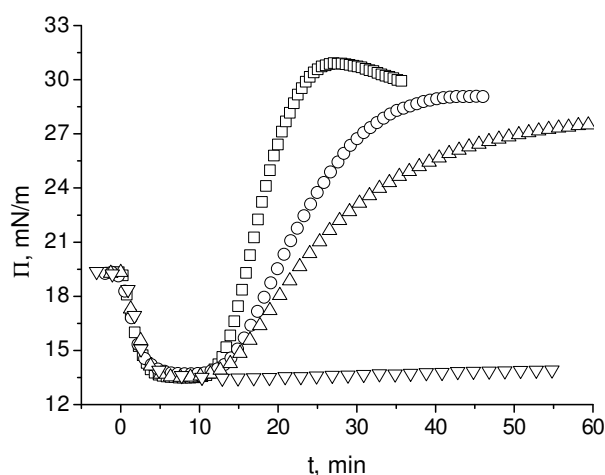

Figure 2. Π-t diagrams depending on initial (vesicular) lipid concentration: $\square$) 63 µM, $\bigcirc$) 42 µM $\triangle$) 21 µM and $\triangledown$) 0 µM. 5 mM $CaCl_2$ were added at t=0 to induce the fusion process.
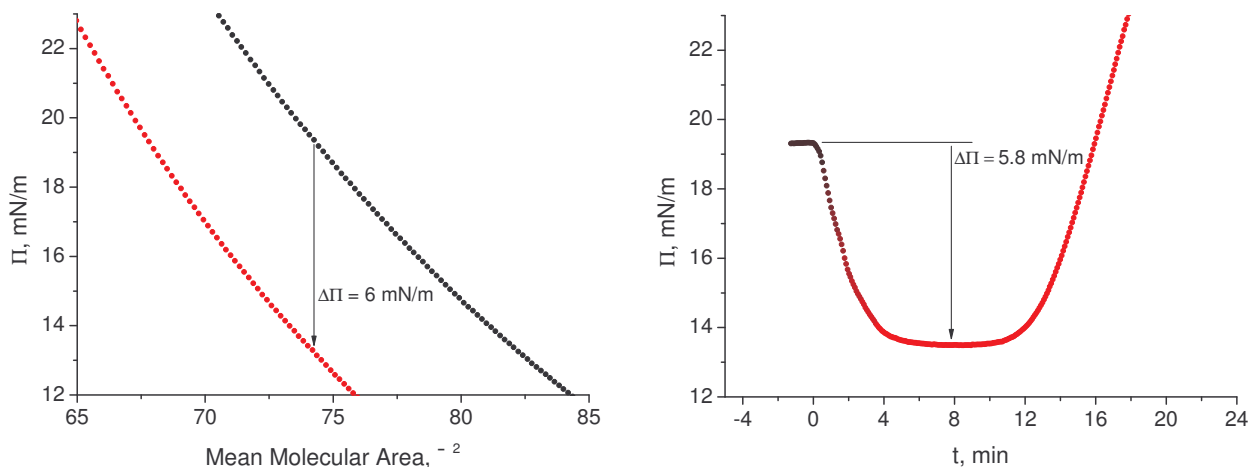
Figure 3. Quantitative comparison between the compression isotherms with and without 5 mM CaCl$_2$ in the subphase and a fusion experiment (POPS/POPC 4:1). The initial pressure is chosen the same. The decrease in surface pressure amounts for 6 mN/m.

The course of $\Pi(t)$ during the pressure decrease (minute 1-5) and the subsequent lag time (minute 5-10) is independent of the vesicle concentration and implies zero lipid transfer from liposomes to a Langmuir film. This behavior can be justified by two considerations; the Ca^{2+} concentration is very large compared to the vesicle concentration, so the subtle differences in liposome concentration do not significantly shift the concentration of free calcium and consequently the association rate between the monolayer and Ca^{2+} ions. In addition, K$_D$ of PS and Ca^{2+} is rather low (ca. 12 M^{-1})[105] and may contribute to the lag-time after the initial condensation effect; the membrane bound calcium needs to exceed a critical concentration to activate fusions.[101]

The successively increasing surface pressure is affected by two factors: the slope is systematically influenced by the vesicle concentration and therefore, as expected, more vesicles increase the lipid transfer rate from vesicles to monolayer. The absence of vesicles served as a negative control: this system does not exhibit any surface pressure increase.

On the other hand, the surface pressure approaches a threshold value at around 30 mN/m and, as measurements with different PS/PC ratios suggest, this critical value does not depend on the vesicle concentration (see 3.2.2). In fact, the interaction of calcium with POPS increases the lateral monolayer rigidity and, as a result, the membrane's POPS proportion determines the threshold pressure of the experiment.[103]

Results from the Π-t isotherms were confirmed by light transmission measurements of liposome solutions, which provide a qualitative insight into the kinetic processes of

aggregation and fusion in the bulk. The increase of the mean object size (aggregates as well as fused vesicles within) was observed by the change of absorption at 600 nm. Given a certain concentration of calcium and PS, the aggregation behavior is related to the mean size of objects, their diffusion coefficient and the mean distance between them.

Varying vesicle concentrations show significantly different growth rates during the first 20 minutes (Figure 4). They are initially the fastest after addition of $CaCl_2$ and proportional to the vesicle concentration and the mean distance between adjacent vesicles, and slow down after ca. 20 minutes to a concentration independent value. This flat part of the curve can be explained by the interplay between the following factors: as the object size increases, diffusion slows down, and the inter-aggregate distances become larger. Therefore, the probability of further aggregation markedly decreases after a certain aggregation number has been reached. The question why this happens approximately at the same time for all investigated lipid concentrations can be answered by two opposing effects being aggregate size and their diffusion speed, directly related to the distance between aggregates. Within a given volume, the initial aggregation is faster at higher liposome concentrations, yet at some point, it becomes equilibrated by the slower motion of these large aggregates, which inhibits their further growth. In addition, proceeding aggregation reduces the membrane area accessible to other aggregates or vesicles and, as a result, decelerates the process of object growth. Reversely, faster object movements will compensate slow aggregation at low lipid concentration.
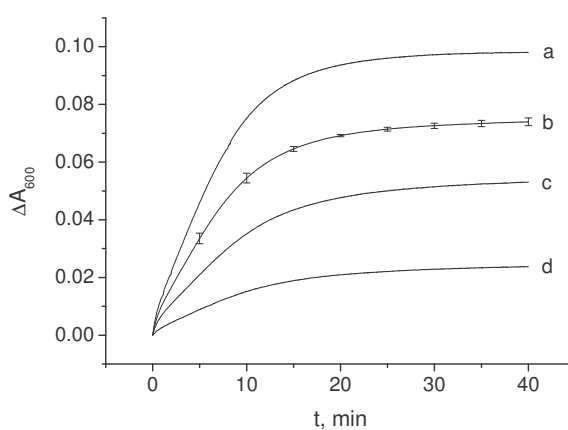

Figure 4. Change of absorption at 600 nm over time. The liposomes consisted of POPS and POPC in a molar ratio of 4:1. The overall lipid concentration was varied as follows: a) 84 μM b) 63 μM c) 42 μM d) 21 μM. The fusion process was induced by addition of 5 mM $CaCl_2$.

Error bars on curve b were calculated as the standard deviation from 5 separate measurements.

To discriminate between the size increase resulting from fusion and aggregation, the process was stopped in intervals of 5 minutes at a time by addition of 10 mM EDTA (curve a in Figure 5). The solution was mixed vigorously with a glass pipette to apply shear force and disrupt residual aggregates, and light transmission measurements were performed. Both (aggregation and fusion) curves are plotted in Figure 5. After addition of EDTA absorption is decreased significantly which suggests the disaggregation of vesicles. This indicates a rate difference between aggregation and fusion; on the other hand, it is evidence for the influence of aggregation on fusion rates. Unlike aggregation, the fusion reaction is not fastest after Ca^{2+} addition. This opposed behavior can be traced back to the total contact area of aggregated vesicles, which is ideally zero at the time of calcium addition, increases as aggregation proceeds and decreases again by ongoing fusion events. This phenomenon is in qualitative agreement with the observation from our surface measurements (Figure 2).
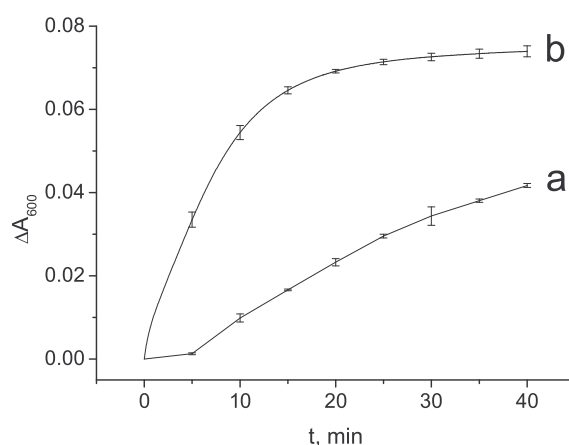

Figure 5. Change of light absorption resulting from aggregation and fusion: overall lipid concentration at both curves is 63 μM. The liposomes consisted of POPS/POPC in a ratio of 4:1. Curve a) was obtained by adding 10 mM EDTA to dissolve vesicle aggregates. Curve b) shows the increase in absorption due to proceeding aggregation and fusion.

3.2.2 Varying Lipid Composition

It is known that shifted molar ratios of POPS and POPC affect the amount of the membrane's negative charge and therefore its fusogenity: fewer PS headgroups will associate to fewer Ca^{2+} ions, decelerate aggregation and therefore slow down the fusion kinetics.[102]

Liposomes of 4:1, 2:1, 1:1, and 1:2 ratios of POPS to POPC were prepared and Π-t isotherms were recorded as described above.

4:1, 1:1 and 1:2 mixtures of POPS/POPC (Figure 6) exhibit a systematic behavior. As expected, the initial decrease of surface pressure after Ca^{2+} addition relates to the molar ratio of POPS to POPC. The higher the PS content the stronger the condensation effect as a response to the Ca^{2+} ions.

For the lipid compositions presented in Figure 6, the rate of mass transport from the bulk to the surface, indicated by the surface pressure increase, relates to the ratio of POPS to POPC.

We observe hardly any fusions of membranes containing 33 % POPS; this is in agreement with the literature where vesicle-vesicle fusions from PS/PC were reported only at PS contents above 40 mole %.[102]

The concentration of calcium ions influences the rate of fusions in PS-containing membranes; at 5 mM Ca^{2+}, a DOPS/DOPC (1,2-dioleoyl-*sn*-glycero-3-phosphocholine; 1,2-dioleoyl-*sn*-glycero-3-[phospho-L-serine]) system is reported to fuse only at PS contents above 58 %[102] (evaluated by a fluorescence assay). In our measurements, the POPS ratio of 50 % was observed to fuse slowly at the same Ca^{2+} concentration, which we attribute mainly to different lipid chemistry. Additionally, fluorescence measurements are confined to short measuring times (in the order of a few minutes) due to increased scattering from growing particles. As indicated by our UV-Vis measurements, fusion rates are not necessarily fastest after Ca^{2+} addition, and may not be detectable at that timescale.
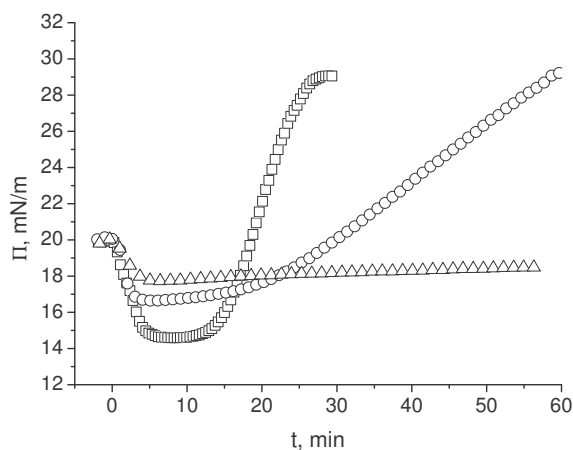
Figure 6. Membrane fusion kinetics for varying lipid compositions. The ratio of POPS to POPC was varied: □) 4:1, ○) 1:1; △) 1:2.

Unlike membranes consisting of 4:1 POPS in POPC, the ratio of 1:1 does not exhibit a threshold pressure of around 30 mN/m but converges to a value of ca. 45 mN/m (not shown). This suggests the threshold is determined by the properties of the Langmuir film; there is evidence that higher ratios of POPS/POPC establish more rigid Langmuir films.[112-114]

The POPS/POPC ratio of 2:1 does not follow the systematic trend described above. The kinetic rate could be expected to fall between the rates for the 1:1 and the 4:1 mixtures, but there is barely any measurable fusion activity (Figure 7, A). Eventually, the fusogenity of POPS/POPC membrane mixtures does not exclusively depend on the amount of negatively charged PS but, to our knowledge, barely anything is known about the system at this particular composition, so there is no established model for its behavior regarding calcium interaction. Phase diagrams obtained from calorimetry data for DMPC/DMPS[102] (1,2-dimyristoyl-sn-glycero-3-phosphocholine; 1,2-dimyristoyl-sn-glycero-3-[phospho-L-serine]) suggest that at this particular ratio the system produces a mixture of solid cochleate phases in the presence of calcium over a wide temperature range. This might apply as well to POPC/POPS: implying only POPS-rich phases responsible for aggregation, the fusion efficiency would be significantly reduced by the presence of solid phases due to restricted lateral lipid mobility.

Nevertheless, the 2:1 mixture tends to aggregate (visible to the naked eye). This observation emerged as a suitable control to exclude the influence of aggregates on the surface pressure and was supplemented by an absorption measurement (Figure 7, B). Comparison with the 1:1 POPS/POPC system illustrates that while both mixtures aggregate, the fused products differ

significantly in size. After addition of EDTA the absorption of 2:1 POPS/POPC vesicles drops to the initial value before Ca^{2+} addition, suggesting that hardly any fusion occurred within at least 40 minutes. Compared to that, the 1:1 mixture readily fuses as indicated by the irreducible size of objects after EDTA addition.
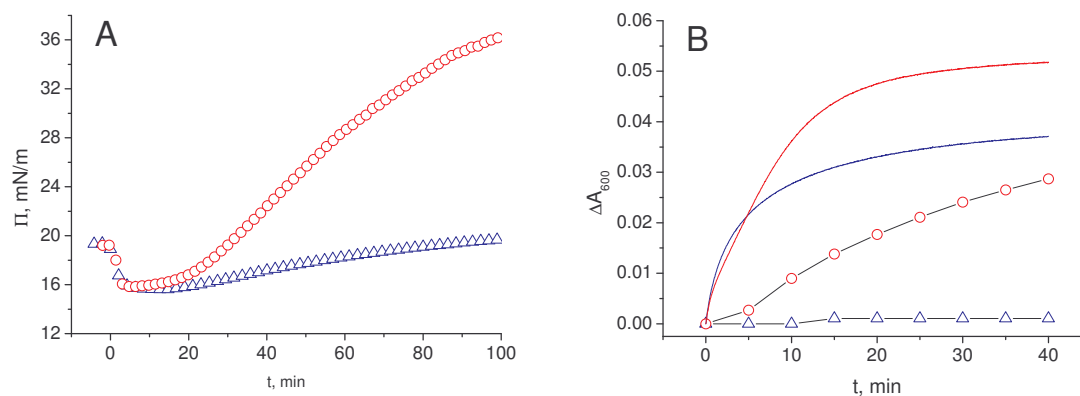
Figure 7. A: Π-t isotherms of POPS/POPC 1:1 (red) and 2:1 (blue) mixtures. Even though there is more negative charge associated to the 2:1 vesicles, they barely fuse upon Ca^{2+} addition. B: Qualitative comparison between aggregation (solid lines) and fusion (open symbols): Barely any fusion between membranes consisting of POPS and POPC in a ratio of 2 to 1.

3.3 Brewster Angle Microscopy

To control the method's selective pressure insensitivity for aggregation, the Langmuir film and the ongoing events directly below the surface were visualized by Brewster angle microscopy, Figure 8. Starting from the time of Ca^{2+} addition bright spots could be observed (Figure 8, a). The number and size of these spots increased in the course of the measurement (Figure 8, b-d) until they started to disappear after EDTA was added (Figure 8, e, f).

We conclude that the spots are aggregates that stick below the surface and did not fuse yet with the lipid monolayer. Concerning the surface pressure changes over that experiment, at first sight it may appear that the initial Π increase is not only related to membrane lipid transport, but also to the presence of these aggregates. On the other hand, as the pressure remained constant over the aggregates' dissolution with EDTA, it is clear that the surface pressure measurement with a Langmuir film balance is not sensitive to liposome aggregation
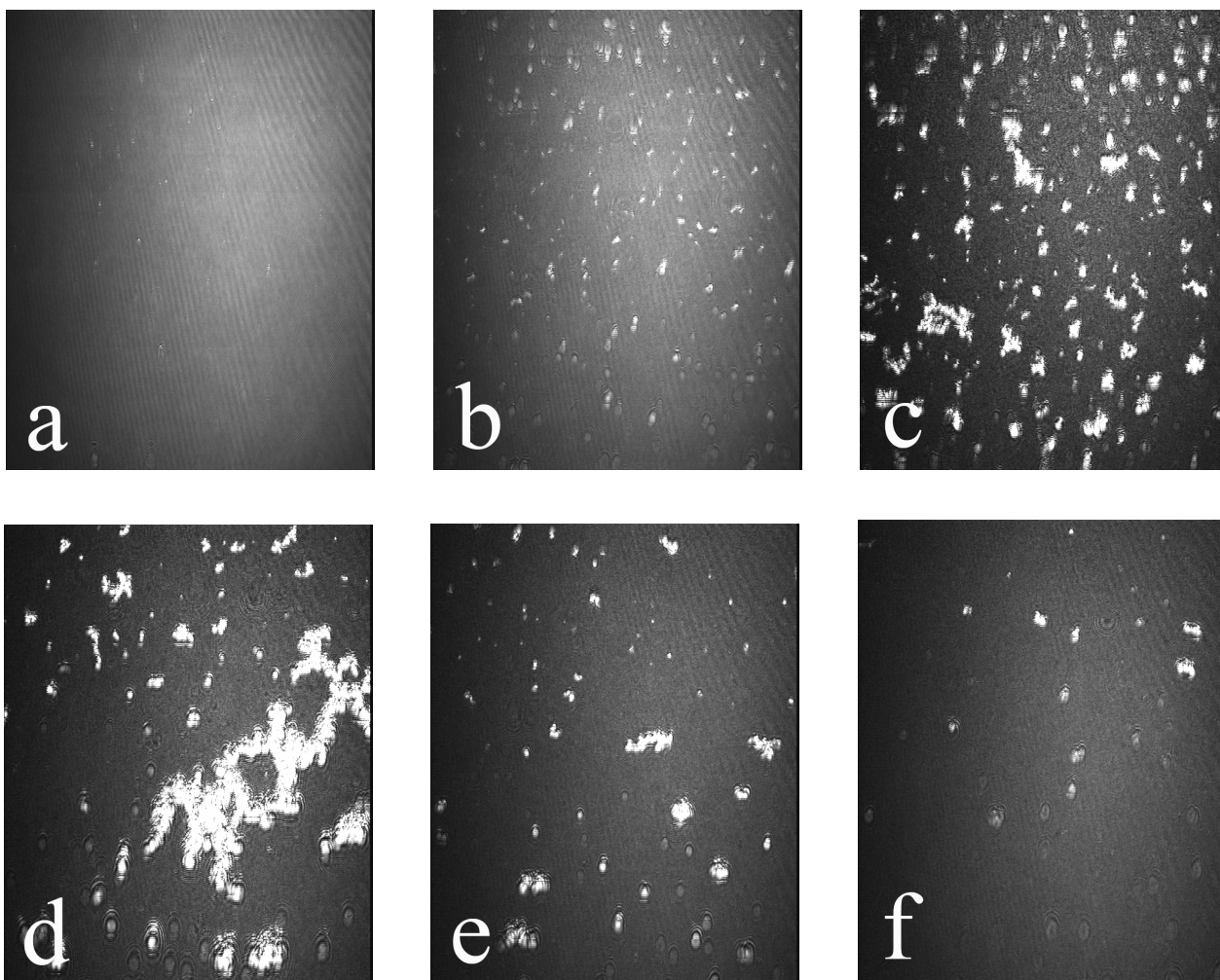
Figure 8. Brewster angle microscopy micrographs from the air-water interface. A lipid monolayer consisting of POPS and POPC in a 4:1 ratio was spread to the initial pressure of 20 mN/m. Picture a) 15 mN/m immediately after addition of 5 mM $CaCl_2$. b) 20 mN/m, c) 24 mN/m, d) 28 mN/m, e) and f) were both taken at 30 mN/m in intervals of 10 minutes after addition of 10 mM EDTA.

3. Conclusions

We applied a Langmuir monolayer technique to measure membrane fusions. Interactions between a lipid film at the air-water interface and lipid vesicles in the bulk were studied by surface pressure changes. Material transfer from the vesicles to the Langmuir film at constant trough area increased the surface pressure, which served as a measure to describe membrane fusions. This work was intended as a feasibility study for reliable and fast evaluation of membrane fusions. Consequently, POPS and POPC lipid mixtures were used as model

membrane components since they represent a well studied fusion system and fuse in response to the presence of calcium ions.

The method allows for studying interactions between membranes of different curvature energies, rather corresponding to in vivo conditions. Moreover, heterologous fusions can easily be studied whenever vesicles and the planar membrane consist of different components.

The influence of changes in vesicle concentration and membrane composition was investigated, and is in agreement with reference data obtained earlier by resonance energy transfer.[102, 115]

There is evidence that our experimental setup is selectively sensitive to fusions and does not respond to aggregation of liposomes below the surface layer, a feature difficult to achieve with other methods. In this context, aggregation reversibility and fusion triggering are instrumental in understanding the process. Additionally, the direct dependency on a physical property (Π) allows for quantifying fusion rates. Calculation of the kinetic constants was not straightforward since, in the case of constant area measurements, they are influenced by the increasing rigidity of the monolayer due to increased surface pressure. This limitation could be overcome by performing the experiments at constant surface pressure. However, while liposomes are present in the bulk, no control can be maintained over their concentration in a conventional Langmuir trough, where a monolayer will be formed[100, 116] and simultaneously compressed outside the barriers.

Unlike cell membranes, Langmuir films in this work were not double layers, so the differences between natural fusion processes and our experimental conditions might be disputed. However, comparison of our data to fusion experiments carried out by means of resonance energy transfer in pure bilayer systems implies a viable applicability of our experimental model. Accordingly, we conclude that the early steps of fusion are not influenced by a second lipid layer. Furthermore, it is noted that our results do not provide any measure for the efficiency of content delivery and have to be supplemented with appropriate assays for these purposes.

With our surface pressure experiments, supplemented further by UV-Vis data and Brewster angle imaging, we believe to have contributed to the current knowledge on quantitative measurements of membrane fusions. With industry likely to apply synthetic (e.g. polymeric) vesicles for drug delivery in near future, this approach may prove a fast and reliable tool for simplifying the empirical description of fusion behavior in both lipid and synthetic membranes.

8 References

1. Forster, S. and T. Plantenberg, *From self-organizing polymers to nanohybrid and biomaterials.* Angewandte Chemie, International Edition, 2002. **41**(5): p. 688-714.

2. Whitesides, G.M. and B. Grzybowski, *Self-assembly at all scales.* Science (Washington, DC, United States), 2002. **295**(5564): p. 2418-2421.

3. Kita-Tokarczyk, K., et al., *Block copolymer vesicles-using concepts from polymer chemistry to mimic biomembranes.* Polymer, 2005. **46**(11): p. 3540-3563.

4. Meier, W., C. Nardin, and M. Winterhalter, *Reconstitution of channel proteins in (polymerized) ABA triblock copolymer membranes.* Angewandte Chemie, International Edition, 2000. **39**(24): p. 4599-4602.

5. Lasie, D.D., *Liposomes: From Physics to Applications*. 1993. 580 pp.

6. Laughlin, R.G., *The Aqueous Phase Behavior of Surfactants*. 1996. 558 pp.

7. Schlaad, H. and M. Antonietti, *Block copolymers with amino acid sequences: Molecular chimeras of polypeptides and synthetic polymers.* European Physical Journal E: Soft Matter, 2003. **10**(1): p. 17-23.

8. Loewik, D.W.P.M. and J.C.M. van Hest, *Peptide based amphiphiles.* Chemical Society Reviews, 2004. **33**(4): p. 234-245.

9. Velonia, K., A.E. Rowan, and R.J.M. Nolte, *Lipase Polystyrene Giant Amphiphiles.* Journal of the American Chemical Society, 2002. **124**(16): p. 4224-4225.

10. Mecke, A., C. Dittrich, and W. Meier, *Biomimetic membranes designed from amphiphilic block copolymers.* Soft Matter, 2006. **2**(9): p. 751-759.

11. Deming, T.J., et al., *Block copolypeptide vesicles and membranes.* Polymeric Materials Science and Engineering, 2004. **90**: p. 302-303.

12. Anfinsen, C.B., *Principles that govern the folding of protein chains.* Prix Nobel, 1973: p. 103-19.

13. Levinthal, C., *How to fold graciously.* Mössbauer spectroscopyin biological systems, 1968.

14. Checot, F., et al., *Water-soluble stimuli-responsive vesicles from peptide-based diblock copolymers.* Angewandte Chemie, International Edition, 2002. **41**(8): p. 1339-1343.

15. Checot, F., et al., *From supramolecular polymersomes to stimuli-responsive nano-capsules based on poly(diene-b-peptide) diblock copolymers.* European Physical Journal E, 2003. **10**(1): p. 25-35.

16. Kimura, S., et al., *Vesicular Self-Assembly of a Helical Peptide in Water.* Langmuir, 1999. **15**(13): p. 4461-4463.

17. Kukula, H., et al., *The formation of polymer vesicles or "peptosomes" by polybutadiene-block-poly(L-glutamate)s in dilute aqueous solution.* Journal of the American Chemical Society, 2002. **124**(8): p. 1658-63.

18. Israelachvili, J.N., *Intermolecular and Surface Forces.* 1991. 291 pp.

19. Boerakker, M.J., et al., *Giant amphiphiles by cofactor reconstitution.* Angewandte Chemie, International Edition, 2002. **41**(22): p. 4239-4241.

20. Fujita, K., S. Kimura, and Y. Imanishi, *Spherical Self-Assembly of a Synthetic a-Helical Peptide in Water.* Langmuir, 1999. **15**(13): p. 4377-4379.

21. Bellomo, E.G., et al., *Stimuli-responsive polypeptide vesicles by conformation-specific assembly.* Nat. Mater., 2004. **3**(4): p. 244-248.

22. Holowka, E.P., D.J. Pochan, and T.J. Deming, *Charged Polypeptide Vesicles with Controllable Diameter.* Journal of the American Chemical Society, 2005. **127**(35): p. 12423-12428.

23. von Maltzahn, G., et al., *Positively charged surfactant-like peptides self-assemble into nanostructures.* Langmuir, 2003. **19**(10): p. 4332-4337.

24. Ye, S., et al., *Amphiphilic 4-Helix Bundles Designed for Biomolecular Materials Applications.* Langmuir, 2004. **20**(14): p. 5897-5904.

25. Hotchkiss, R.D. and R. Dubos, *Fractionation of the bactericidal agent from cultures of a soil bacillus.* Journal of Biological Chemistry, 1940. **132**: p. 791-2.

26. Hotchkiss, R.D. and R. Dubos, *Chemical properties of bactericidal substances isolated from cultures of a soil bacillus.* Journal of Biological Chemistry, 1940. **132**: p. 793-4.

27. Andersen Olaf, S., E. Koeppe Roger, 2nd, and B. Roux, *Gramicidin channels.* IEEE Trans Nanobioscience FIELD Full Journal Title:IEEE transactions on nanobioscience, 2005. **4**(1): p. 10-20.

28. Roux, B. and M. Karplus, *Ion transport in a gramicidin-like channel: dynamics and mobility.* Journal of Physical Chemistry, 1991. **95**(12): p. 4856-68.

29. Olah, G.A., et al., *Location of ion-binding sites in the gramicidin channel by x-ray diffraction.* Journal of Molecular Biology, 1991. **218**(4): p. 847-58.

30.   Wallace, B.A., W.R. Veatch, and E.R. Blout, *The effects of lipid environment, ion-binding and chemical modifications on the structure of the gramicidin transmembrane channel.* Biophysical Journal, 1982. **37**(1): p. 197-9.

31.   Chen, Y. and B.A. Wallace, *The effects of calcium ions on double helical forms of gramicidin.* European Biophysics Journal, 1997. **26**(4): p. 299-306.

32.   Bamberg, E., H.J. Apell, and H. Alpes, *Structure of the gramicidin A channel: Discrimination between the pL,D and the b helix by electrical measurements with lipid bilayer membranes.* Proceedings of the National Academy of Sciences of the United States of America, 1977. **74**(6): p. 2402-6.

33.   Weinstein, S., et al., *Conformation of the gramicidin A transmembrane channel. A carbon-13 nuclear magnetic resonance study of carbon-13-enriched gramicidin in phosphatidylcholine vesicles.* Journal of Molecular Biology, 1980. **143**(1): p. 1-19.

34.   Wallace, B.A., *Gramicidin A adopts distinctly different conformations in membranes and in organic solvents.* Biopolymers, 1983. **22**(1): p. 397-402.

35.   Weinstein, S., et al., *Conformation of gramicidin A channel in phospholipid vesicles: A carbon-13 and fluorine-19 nuclear magnetic resonance study.* Proceedings of the National Academy of Sciences of the United States of America, 1979. **76**(9): p. 4230-4.

36.   Wallace, B.A. and R.W. Janes, *Co-crystals of gramicidin A and phospholipid. A system for studying the structure of a transmembrane channel.* Journal of Molecular Biology, 1991. **217**(4): p. 625-7.

37.   Wallace, B.A., *Recent advances in the high resolution structures of bacterial channels: gramicidin A.* Journal of Structural Biology, 1998. **121**(2): p. 123-141.

38.   Veatch, W.R., E.T. Fossel, and E.R. Blout, *Conformation of gramicidin A.* Biochemistry, 1974. **13**(26): p. 5249-56.

39.   Urry, D.W., D.F. Mayers, and J. Haider, *Spectroscopic studies on the conformation of gramicidin A'. Evidence for a new helical conformation.* Biochemistry, 1972. **11**(4): p. 487-93.

40.   Heitz, F., A. Heitz, and Y. Trudelle, *Conformations of gramicidin A and its 9,11,13,15-phenylalanyl analog in dimethyl sulfoxide and chloroform.* Biophys Chem FIELD Full Journal Title:Biophysical chemistry, 1986. **24**(2): p. 149-60.

41.   Urry, D.W., et al., *Conformation and molecular mechanisms of carriers and channels.* Annals of the New York Academy of Sciences, 1975. **264**(Carriers Channels Biol. Syst.): p. 203-20.

42.   Sychev, S.V., et al., *The solution conformations of gramicidin A and its analogs.* Bioorganic Chemistry, 1980. **9**(1): p. 121-51.

43.   Chen, Y., A. Tucker, and B.A. Wallace, *Solution structure of a parallel left-handed double-helical gramicidin-A determined by 2D 1H NMR.* Journal of Molecular Biology, 1996. **264**(4): p. 757-769.

44.   Doyle, D.A. and B.A. Wallace, *Crystal structure of the gramicidin/potassium thiocyanate complex.* Journal of Molecular Biology, 1997. **266**(5): p. 963-977.

45.   Hladky, S.B. and D.A. Haydon, *Discreteness of conductance change in bimolecular lipid membranes in the presence of certain antibiotics.* Nature (London, United Kingdom), 1970. **225**(5231): p. 451-3.

46.   Hladky, S.B. and D.A. Haydon, *Ion transfer across lipid membranes in the presence of gramicidin A. I. Unit conductance channel.* Biochimica et Biophysica Acta, Biomembranes, 1972. **274**(2): p. 294-312.

47.   Bamberg, E., et al., *Single-channel parameters of gramicidin A,B, and C.* Biochim Biophys Acta FIELD Full Journal Title:Biochimica et biophysica acta, 1976. **419**(2): p. 223-8.

48.   Eisenman, G., J. Sandblom, and E. Neher, *Interactions in cation permeation through the gramicidin channel. Cs, Rb, K, Na, Li, Tl, H, and effects of anion binding.* Biophys J FIELD Full Journal Title:Biophysical journal, 1978. **22**(2): p. 307-40.

49.   Urry, D.W., *The gramicidin A transmembrane channel: a proposed pi(L,D) helix.* Proc Natl Acad Sci U S A FIELD Full Journal Title:Proceedings of the National Academy of Sciences of the United States of America, 1971. **68**(3): p. 672-6.

50.   Wallace, B.A., *Structure of gramicidin A.* Biophysical journal, 1986. **49**(1): p. 295-306.

51.   Masotti, L., A. Spisni, and D.W. Urry, *Conformational studies on the gramicidin A transmembrane channel in lipid micelles and liposomes.* Cell Biophys FIELD Full Journal Title:Cell biophysics, 1980. **2**(3): p. 241-51.

52.   Tournois, H., et al., *Solvent determined conformation of gramicidin affects the ability of the peptide to induce hexagonal HII phase formation in*

dioleoylphosphatidylcholine model membranes. Biochim Biophys Acta FIELD Full Journal Title:Biochimica et biophysica acta, 1987. **905**(1): p. 222-6.

53.   Wallace, B.A., *Ion-bound forms of the gramicidin A transmembrane channel.* Biophysical Journal, 1984. **45**(1): p. 114-16.

54.   Shungu, D.C., et al., *Investigation of the interaction between thallous ions and gramicidin A in dimyristoylphosphatidylcholine vesicles: a thallium-205 NMR equilibrium study.* Biochemistry FIELD Full Journal Title:Biochemistry, 1986. **25**(20): p. 6103-8.

55.   Koeppe, R.E., II and O.S. Andersen, *Engineering the gramicidin channel.* Annual Review of Biophysics and Biomolecular Structure, 1996. **25**: p. 231-258.

56.   Wallace, B.A., *Gramicidin channels and pores.* Annual Review of Biophysics and Biophysical Chemistry, 1990. **19**: p. 127-57.

57.   Andersen, O.S., *Kinetics of ion movement mediated by carriers and channels.* Methods Enzymol FIELD Full Journal Title:Methods in enzymology, 1989. **171**: p. 62-112.

58.   Busath, D.D., *The use of physical methods in determining gramicidin channel structure and function.* Annual Review of Physiology, 1993. **55**: p. 473-501.

59.   Wallace, B.A., *Crystallographic studies of a transmembrane ion channel, gramicidin A.* Progress in Biophysics & Molecular Biology, 1992. **57**(2): p. 59-69.

60.   Roux, B. and M. Karplus, *Molecular dynamics simulations of the gramicidin channel.* Annual Review of Biophysics and Biomolecular Structure, 1994. **23**: p. 731-61.

61.   Pullman, A., *Contribution of theoretical chemistry to the study of ion transport through membranes.* Chemical Reviews (Washington, DC, United States), 1991. **91**(5): p. 793-812.

62.   Killian, J.A., *Gramicidin and gramicidin-lipid interactions.* Biochim Biophys Acta FIELD Full Journal Title:Biochimica et biophysica acta, 1992. **1113**(3-4): p. 391-425.

63.   Doyle, D.A. and B.A. Wallace. *The dynamic nature of gramicidin*. 1996.

64.   Doyle, D.A. and B.A. Wallace, *Shifting the equilibrium mixture of gramicidin double helices toward a single conformation with multivalent cationic salts.* Biophysical journal, 1998. **75**(2): p. 635-40.

65.   Isbell, B.E., C. Rice-Evans, and G.H. Beaven, *Conformation of gramicidin A in solution.* FEBS Letters, 1972. **25**(1): p. 192-6.

66.   Bystrov, V. and A. Arsen'ev. *NMR of gramicidin A double helices*. 1985.

67.   Pascal, S.M. and T.A. Cross, *High-resolution structure and dynamic implications for a double-helical gramicidin A conformer.* Journal of Biomolecular NMR, 1993. **3**(5): p. 495-513.

68.   Bouchard, M., J.H. Davis, and M. Auger, *High-speed magic angle spinning solid-state 1H nuclear magnetic resonance study of the conformation of gramicidin A in lipid bilayers.* Biophys J FIELD Full Journal Title:Biophysical journal, 1995. **69**(5): p. 1933-8.

69.   Cotten, M., F. Xu, and T.A. Cross, *Protein stability and conformational rearrangements in lipid bilayers: linear gramicidin, a model system.* Biophysical Journal, 1997. **73**(2): p. 614-623.

70.   Pascal, S.M. and T.A. Cross, *Structure of an isolated gramicidin A double helical species by high-resolution nuclear magnetic resonance.* Journal of Molecular Biology, 1992. **226**(4): p. 1101-9.

71.   Langs, D.A., *Three-dimensional structure at 0.86 .ANG. of the uncomplexed form of the transmembrane ion channel peptide gramicidin A.* Science (Washington, DC, United States), 1988. **241**(4862): p. 188-91.

72.   Wallace, B.A. and K. Ravikumar, *The gramicidin pore: crystal structure of a gramicidin/cesium chloride complex.* Jerusalem Symposia on Quantum Chemistry and Biochemistry, 1988. **21**(Transp. Membr.: Carriers, Channels Pumps): p. 103-13.

73.   Arseniev, A.S., I.L. Barsukov, and V.F. Bystrov, *NMR solution structure of gramicidin A complex with cesium cations.* FEBS Letters, 1985. **180**(1): p. 33-9.

74.   Lomize, A.L., V.Y. Orekhov, and A.S. Arsen'ev, *Refinement of the spatial structure of the gramicidin A transmembrane ion-channel.* Bioorganicheskaya Khimiya, 1992. **18**(2): p. 182-200.

75.   Ketchem, R.R., B. Roux, and T.A. Cross. *Computational refinement through solid state NMR and energy constraints of a membrane bound polypeptide.* 1996.

76.   Wallace, B.A. and K. Ravikumar, *The gramicidin pore: crystal structure of a cesium complex.* Science (Washington, DC, United States), 1988. **241**(4862): p. 182-7.

77.   Arseniev, A.S., et al., *1H-NMR study of gramicidin A transmembrane ion channel. Head-to-head right-handed, single-stranded helices.* FEBS Lett FIELD Full Journal Title:FEBS letters, 1985. **186**(2): p. 168-74.

78.   Veatch, W.R. and E.R. Blout, *Aggregation of gramicidin A in solution.* Biochemistry, 1974. **13**(26): p. 5257-64.

79.   Roux, B., R. Bruschweiler, and R.R. Ernst, *The structure of gramicidin A in dimethylsulfoxide/acetone.* Eur J Biochem FIELD Full Journal Title:European journal of biochemistry / FEBS, 1990. **194**(1): p. 57-60.

80.   Chen, Y. and B.A. Wallace, *Solvent effects on the conformation and far UV CD spectra of gramicidin.* Biopolymers, 1997. **42**(7): p. 771-781.

81.   Zhang, Z., S.M. Pascal, and T.A. Cross, *A conformational rearrangement in gramicidin A: From a double-stranded left-handed to a single-stranded right-handed helix.* Biochemistry, 1992. **31**(37): p. 8822-8.

82.   Killian, J.A., et al., *The membrane as an environment of minimal interconversion. A circular dichroism study on the solvent dependence of the conformational behavior of gramicidin in diacylphosphatidylcholine model membranes.* Biochemistry, 1988. **27**(13): p. 4848-55.

83.   Macdonald, P.M. and J. Seelig, *Dynamic properties of gramicidin A in phospholipid membranes.* Biochemistry, 1988. **27**(7): p. 2357-64.

84.   Nekrasov, A.N., A.V. Stepanov, and V.P. Timofeev, *The features of the spatial structure of the gramicidine A-cesium complex.* FEBS Letters, 1995. **371**(1): p. 35-8.

85.   Gibson, G.A. and L.M. Loew, *Phospholipid vesicle fusion monitored by fluorescence energy transfer.* Biochemical and Biophysical Research Communications, 1979. **88**(1): p. 135-40.

86.   Fung, B.K.-K. and L. Stryer, *Surface density determination in membranes by fluorescence energy transfer.* Biochemistry, 1978. **17**(24): p. 5241-8.

87.   Struck, D.K., D. Hoekstra, and R.E. Pagano, *Use of resonance energy transfer to monitor membrane fusion.* Biochemistry, 1981. **20**(14): p. 4093-9.

88.   Ellens, H., J. Bentz, and F.C. Szoka, *Proton- and calcium-induced fusion and destabilization of liposomes.* Biochemistry, 1985. **24**(13): p. 3099-106.

89. Wilschut, J., et al., *Studies on the mechanism of membrane fusion: kinetics of calcium ion induced fusion of phosphatidylserine vesicles followed by a new assay for mixing of aqueous vesicle contents.* Biochemistry, 1980. **19**(26): p. 6011-21.

90. Wilschut, J. and D. Papahadjopoulos, *Ca2+-induced fusion of phospholipid vesicles monitored by mixing of aqueous contents.* Nature, 1979. **281**(5733): p. 690-2.

91. Nir, S., J. Bentz, and J. Wilschut, *Mass action kinetics of phosphatidylserine vesicle fusion as monitored by coalescence of internal vesicle volumes.* Biochemistry, 1980. **19**(26): p. 6030-6.

92. Selvin, P.R., *Fluorescence resonance energy transfer.* Methods in Enzymology, 1995. **246**: p. 300-34.

93. Stryer, L. and R.P. Haugland, *Energy transfer. Spectroscopic ruler.* Proceedings of the National Academy of Sciences of the United States of America, 1967. **58**(2): p. 719-26.

94. Duzgunes, N., et al., *Lipid mixing during membrane aggregation and fusion: why fusion assays disagree.* Biochemistry, 1987. **26**(25): p. 8435-42.

95. Hofmann, M.W., et al., *De novo design of conformationally flexible transmembrane peptides driving membrane fusion.* Proceedings of the National Academy of Sciences of the United States of America, 2004. **101**(41): p. 14776-14781.

96. Nunes-Correia, I., et al., *Fluorescent probes for monitoring virus fusion kinetics: comparative evaluation of reliability.* Biochimica Et Biophysica Acta-Biomembranes, 2002. **1561**(1): p. 65-75.

97. Schindler, H., *Exchange and interactions between lipid layers at the surface of a liposome solution.* Biochimica et biophysica acta, 1979. **555**(2): p. 316-36.

98. Mitev, D.J., T. Ivanova, and C.S. Vassilieff, *Kinetics of lipid layer formation at interfaces.* Colloids And Surfaces B-Biointerfaces, 2002. **24**(3-4): p. 185-192.

99. Gugliotti, M., H. Chaimovich, and M.J. Politi, *Fusion of vesicles with the air-water interface: the influence of polar head group, salt concentration, and vesicle size.* Biochimica Et Biophysica Acta-Biomembranes, 2000. **1463**(2): p. 301-306.

100. Fenzl, W., et al., *The Surface-Confined Structures Of Dimyristoylphosphatidylcholine Bilayers In Contact With The Vesicle*

Suspension As Studied By Means Of X-Ray Reflectivity. Colloids And Surfaces A-Physicochemical And Engineering Aspects, 1995. **102**: p. 247-256.

101. Bentz, J. and N. Duezguenes, *Fusogenic capacities of divalent cations and effect of liposome size.* Biochemistry, 1985. **24**(20): p. 5436-43.

102. Silvius, J.R. and J. Gagne, *Calcium-induced fusion and lateral phase separations in phosphatidylcholine-phosphatidylserine vesicles. Correlation by calorimetric and fusion measurements.* Biochemistry, 1984. **23**(14): p. 3241-7.

103. Marsh, D., *Lateral pressure in membranes.* Biochimica et Biophysica Acta, 1996. **1286**(3): p. 183-223.

104. Wilschut, J., N. Duzgunes, and D. Papahadjopoulos, *Calcium/magnesium specificity in membrane fusion: kinetics of aggregation and fusion of phosphatidylserine vesicles and the role of bilayer curvature.* Biochemistry, 1981. **20**(11): p. 3126-33.

105. McLaughlin, S., et al., *Adsorption of divalent cations to bilayer membranes containing phosphatidylserine.* Journal of General Physiology, 1981. **77**(4): p. 445-73.

106. Ohki, S., N. Duzgunes, and K. Leonards, *Phospholipid vesicle aggregation: effect of monovalent and divalent ions.* Biochemistry, 1982. **21**(9): p. 2127-33.

107. Ohki, S., *A mechanism of divalent ion-induced phosphatidylserine membrane fusion.* Biochimica et Biophysica Acta, 1982. **689**(1): p. 1-11.

108. Hoekstra, D., *Role of lipid phase separations and membrane hydration in phospholipid vesicle fusion.* Biochemistry, 1982. **21**(12): p. 2833-40.

109. Li, M., U. Retter, and J. Lipkowski, *Kinetic Studies of Spreading DMPC Vesicles at the Air-Solution Interface Using Film Pressure Measurements.* Langmuir, 2005. **21**(10): p. 4356-4361.

110. Papahadjopoulos, D., *Surface properties of acidic phospholipids: interaction of monolayers and hydrated liquid crystals with uni- and bi-valent metal ions.* Biochimica et biophysica acta, 1968. **163**(2): p. 240-54.

111. Rojas, E. and J.M. Tobias, *Membrane Model: Association Of Inorganic Cations With Phospholipid Monolayers.* Biochimica et biophysica acta, 1965. **94**: p. 394-404.

112. Rhodes, D.G. and J. Liu, *Divalent cation mediated binding of oligonucleotides to Langmuir monolayers of charged lipids.* Langmuir, 1996. **12**(7): p. 1879-1883.

113. Mattai, J., et al., *Interactions Of Metal-Ions With Phosphatidylserine Bilayer-Membranes - Effect Of Hydrocarbon Chain Unsaturation.* Biochemistry, 1989. **28**(5): p. 2322-2330.

114. Gamsjaeger, R., et al., *Membrane binding of b2-glycoprotein I can be described by a two-state reaction model: an atomic force microscopy and surface plasmon resonance study.* Biochemical Journal, 2005. **389**(3): p. 665-673.

115. Nir, S., J. Wilschut, and J. Bentz, *The rate of fusion of phospholipid vesicles and the role of bilayer curvature.* Biochimica et Biophysica Acta, 1982. **688**(1): p. 275-8.

116. Lawrie, G.A., G.T. Barnes, and I.R. Gentle, *Self-assembled films of dimyristoylphosphatidylcholine.* Colloids and Surfaces, A: Physicochemical and Engineering Aspects, 1999. **155**(1): p. 69-84.

9 Curriculum Vitae

Personal Details

Name	Christian Dittrich
Date and place of birth	21-12-76 Liestal, Switzerland
Nationality / Permit	German / C

Education

University of Basel	Ph.D. under the supervision of Prof. Dr. W. Meier.	
	Focus: Membrane self-assembly of short peptides	2003-2007
Biozentrum Basel	Master thesis under the supervision of	
	Prof. Dr. T. Kiefhaber. Focus: Protein folding	2002-2003
University of Bern	Master degree in chemistry	1998-2003
High School	Basel, Gymnasium BZB, Eidg. Matur Typus E	1995-1998

References

Prof. Wolfgang Meier	University of Basel	+41 61 26 72156
Dr. Hans Mechler	DSM (Licensing)	+41 61 68 78768
Harry Gubelmann	DSM (Business Intelligence)	+41 61 68 88165